Unified View of Sediment Transport by Currents and Waves. I: Initiation of Motion, Bed Roughness, and Bed-Load Transport

Leo C. van Rijn[1]

Abstract: Attention is given to the properties of sediment beds over the full range of conditions (silts to gravel), in particular the effect of fine silt on the bed composition and on initiation of motion (critical conditions) is discussed. High-quality bed-load transport data sets are identified and analyzed, showing that the bed-load transport in the sand range is related to velocity to power 2.5. The bed-load transport is not much affected by particle size. The prediction of bed roughness is addressed and the prediction of bed-load transport in steady river flow is extended to coastal flow applying an intrawave approach. Simplified bed-load transport formulas are presented, which can be used to obtain a quick estimate of bed-load transport in river and coastal flows. It is shown that the sediment transport of fine silts to coarse sand can be described in a unified model framework using fairly simple expressions. The proposed model is fully predictive in the sense that only the basic hydrodynamic parameters (depth, current velocity, wave height, wave period, etc.) and the basic sediment characteristics (d_{10}, d_{50}, d_{90}, water temperature, and salinity) need to be known. The prediction of the effective bed roughness is an integral part of the model.

DOI: 10.1061/(ASCE)0733-9429(2007)133:6(649)

CE Database subject headings: Sediment transport; Bed roughness; Velocity; Bed load; Silts; Currents.

Introduction

The collective movement of solid particles, known as sediment transport, along a natural bed of the same sediment material is a complex, but intriguing problem which one can only hope to solve at some time. As the sediment transport problem is strongly related to the generation and migration of bed forms such as ripples and dunes, these phenomena are part of the problem and should be included in some way in a rational theory. Historical overviews of the complicated sediment transport and bed roughness problem are given by Graf (1971), Vanoni (1975), and Yalin (1977) for the river regime and by Sleath (1984), Nielsen (1992), Fredsøe and Deigaard (1992), Soulsby (1997), and van Rijn (1993, 2007) for the coastal regime. These works show important facts about the differences between wave environments and current environments and between the different bed form regimes.

In his early research the author (van Rijn 1984a,b,c) has focused on sediment transport and bed roughness in steady river flow. Using a diffusion type of approach, a set of equations has been proposed to describe the near-bed concentration and the vertical distribution of the sediment concentrations over the depth. The method was tested over a range of flow and sediment conditions using both laboratory and field data and shown to work well. From 1984 onwards the method was gradually improved and extended to coastal flow conditions with combined quasi-steady (tidal) flow and surface waves. The progress was slow because field data sets essential for the verification of new theories were extremely scarce. Owing to the perseverance of many field workers around the world to collect sediment transport data in stormy coastal waters, new data sets have become available during recent years for testing and improvement of theoretical modeling work.

The depth-integrated sediment transport is herein defined to consist of: (1) bed-load transport, which is the transport of sediment particles in a thin layer with thickness δ close to the bed (of the order of 0.01 m); and (2) suspended load transport, which is the transport of sediment particles above the bed-load layer.

The suspended load transport can be determined by depth integration of the product of sediment concentration and fluid velocity from the top of the bed-load layer ($z=\delta$) to the water surface. The total sediment transport is obtained as the sum of the net bed load (q_b) and net suspended load (q_s) transport rates, as follows: $q_{tot}=q_b+q_s$ In the presence of surface waves the total transport is defined as the net transport averaged over the wave period. For practical reasons the suspended transport will be subdivided in current-related and wave-related transport components.

In this series of papers it will be shown that the sediment transport of fine silts to coarse sand and gravel can be described in a unified model framework using fairly simple expressions. The proposed model is fully predictive in the sense that only the basic hydrodynamic parameters (depth, current velocity, wave height, wave period, etc.) and the basic sediment characteristics (d_{10}, d_{50}, d_{90}, water temperature, and salinity) need to be known. The prediction of the effective bed roughness will be an integral part of the model. The model consisting of bed load and suspended load transport is an update of the TRANSPOR1993 model and will be referred to as the TRANSPOR2004 model (the abbreviation TR2004 will be used herein).

In this Part 1 new approaches are introduced with respect to

[1]Professor, Delft Hydraulics and Univ. of Utrecht, P.O. Box 177, Delft 2600 MH, The Netherlands. E-mail: leo.vanrijn@wldelft.nl

Note. Discussion open until November 1, 2007. Separate discussions must be submitted for individual papers. To extend the closing date by one month, a written request must be filed with the ASCE Managing Editor. The manuscript for this paper was submitted for review and possible publication on July 8, 2005; approved on August 2, 2006. This paper is part of the ***Journal of Hydraulic Engineering***, Vol. 133, No. 6, June 1, 2007. ©ASCE, ISSN 0733-9429/2007/6-649–667/$25.00.

Table 1. Types of Sand–Mud Mixtures

Type of sediment	Percentage of organic material (%)	Percentage of clay+fine silt (<8 μm) (%)	Percentage of silt (8–62 μm) (%)	Percentage of sand (>62 μm) (%)
Sand (noncohesive)	0	0	0	100
Muddy sand (weakly cohesive)	0–10	0–5	20–40	60–80
Sandy mud (cohesive)	0–10	5–10	30–60	60–30
Mud (cohesive)	0–20	10–20	50–70	0–10
Silty mud (cohesive)	0–20	10–40	60–80	0
Clayey mud (cohesive)	0–20	40–60	40–60	0

the effect of fine silt on the bed composition and on initiation of motion (critical conditions), the prediction of bed roughness and bed-load transport in combined steady and oscillatory flow is dressed. Finally, a simplified bed-load transport formula is presented, which can be used to obtain a quick estimate of bed-load transport in river and coastal flows.

Sediment Bed Classification and Transport Processes

The grain size scale of the American Geophysical Union for sediments with particle sizes smaller than 2 mm consists of about 13 subclasses ranging from very coarse sand to very fine clay. Herein, five somewhat broader subclasses are distinguished:

- Coarse sand (noncohesive) 0.5–2 mm (500–2000 μm);
- Fine sand (noncohesive) 0.062–0.5 mm (62–500 μm);
- Coarse silt (sometimes cohesive) 0.032–0.062 mm (32–62 μm);
- Fine silt (weakly cohesive) 0.08–0.032 mm (8–32 μm); and
- Clay+very fine silt (very cohesive) <0.08 mm (<8 μm).

The following class separation diameters are herein used: d_{gravel} =2,000 μm, d_{sand}=62 μm, d_{silt}=32 μm, and d_{cs}=8 μm. Basically, the pure clay fraction is the fraction with sediments smaller than 2 μm (lutum). For practical reasons (laboratory determination of the percentage <2 μm is extremely difficult), the cohesive fraction with clay and very fine silt is herein defined to consist of particles with diameters smaller than 8 μm (clay-dominated fraction). Bed samples consisting of mixtures of clay, silt, and sand are herein classified as: mud, sandy mud, silty mud, or clayey mud, depending on the percentages of sand, silt, clay, and organic material (Table 1).

The transport of bed material particles may be in the form of either bed-load or bed-load plus suspended load, depending on the size of the bed material particles and the flow conditions. The suspended load may also include some wash load (usually, clay-dominated fraction smaller than 8 μm).

In major rivers the clay-dominated fraction with particle sizes smaller than about 8 μm can hardly be observed in bed material samples indicating that there is not much exchange of this fraction with the bed. Therefore the presence of this very fine sediment fraction in the water is herein defined as the wash load determined by upstream supply conditions. Bagnold (1962) has shown that the very fine fraction can be transported in almost unlimited quantities (autosuspension) depending on the supply rate of very fines to the river by soil erosion and surface runoff. In the absence of reservoirs the majority of the bed material load and the wash load will be transported to the mouth of the river (estuary) where it will be deposited at the mouth bed. Generally, a distinct downstream fining pattern from sand to clay can be observed along the bed of the estuaries (Li et al. 1993). At the most distal locations in the estuary where there is a transition from fresh to saline water (turbidity maximum) and where the tide is dominant, the bed usually consists of very fine cohesive sediments (mud). Under the dominant regime of tidal motion superimposed by surface waves during windy conditions a continuous cycle of deposition, consolidation, fluidization, erosion, flocculation, and deposition and so on of fine sediments is established in strong interaction with the prevailing mud bed.

In the lower river reaches and in most tidal basins the sediments are generally deposited in distinct patterns of sand (channels), silt, and clay (flats). The deposits (flats) of fines in shallow water generally consist of thin layers of clay, silt, and fine sand; the clay and silt fractions being the dominant fractions. Mixing may take place by biological processes. The presence of these different types of sediment (clay, silt, and sand) in the system will result in selective transport processes (particle sorting). This latter process is related to the selective movement of different types of sediment particles near incipient motion at low bed-shear stresses and during generalized transport at higher shear stresses. Sorting effects can only be represented by taking into account the full size composition of the bed material, which may vary horizontally and vertically (see Part 3).

The sand, silt, and clay mixture (on the flats) generally behaves as a mixture with cohesive properties when the clay–silt fraction (<62 μm; herein defined as the mud content including organic materials) is dominant (>0.3) and as a noncohesive mixture when the sand fraction is dominant (>0.7). The distinction between noncohesive mixtures and cohesive mixtures can be related to a critical clay–silt or mud content ($p_{\text{cs,cr}}$). Most important is the value of the clay-dominated fraction (<8 μm) in the mixture. Cohesive properties become dominant when the clay-dominated fraction is larger than about 5–10%. Assuming a clay–silt ratio of 0.5 to 0.25 for natural beds (Van Ledden 2003), the critical clay–silt content will be about $p_{\text{cs,cr}}$=0.2–0.4.

If the mud content is below the critical value ($p_{\text{cs}}<p_{\text{cs,cr}}$), the bed is herein assumed to be homogeneous with depth and to behave as a sand bed with weak cohesive or noncohesive properties. The erosion of the sand particles is the dominant erosion mechanism and the clay–silt particles will be washed out together with the sand particles. Laboratory and field observations (van Rijn 1993, 2005, and Van Ledden 2003) have shown that the erosion or pickup process of the sand particles is slowed down by the presence of the clay–silt particles. This behavior can be quite well modeled by increasing the critical bed-shear stress for initiation of motion of the sand particles.

A fully cohesive bed is different from a noncohesive bed in the sense that the density of the bed is not constant in time due to hindered settling and consolidation processes taking place in the near-bed region. Particle–particle interaction of very fine cohesive particles results in aggregation (flocs) of the particles. In the final stage of the (hindered) settling process near the bed these flocs become space filling and form a network structure (gelling structure), which is the onset of the consolidation process (Winterwerp 1999, 2001). The concentration at the transition from hindered settling to consolidation (or from mobile fluid mud to immobile consolidating mud) is defined as the gelling concentration c_{gel}. Herein, it is tentatively proposed that the gelling concentration can be described by

$$c_{gel} = (d_{50}/d_{sand})^{\alpha} c_{gel,s} \quad \text{with } c_{min} = 0.05 \text{ (volume)} \tag{1}$$

where d_{50}=median particle of bed (range of 4–62 μm); d_{sand} =62 μm=smallest particle size of noncohesive bed (sand); $c_{gel,s}$ =(1−η)=0.65=dry bulk density of sand bed by volume [or=(1 −η)ρ_s=1,722 kg/m^3 as dry bulk density by mass], ρ_s=sediment density; η=porosity of sand bed (≅0.35 for pure sand bed); and α=empirical coefficient (assumed to be α=1 herein). Eq. (1) yields c_{gel}=0.1 (or 270 kg/m^3) for a mud bed of 10 μm and c_{gel}=0.05 (or 130 kg/m^3) for a mud bed of 4 μm, the latter value (c_{gel}=0.05) is herein used as the minimum value. These values are in reasonably good agreement with observations at the mouth of the Amazon in Brazil (Vinzon and Mehta 2003). They have made detailed concentration and velocity measurements through the mobile fluid mud layer. The gelling/maximum concentrations at the bottom of the mobile hyperpycnal layer were of the order of 200–250 kg/m^3. Just above the immobile bed the sediment concentrations were of the order of 200 kg/m^3 decreasing to about 10 kg/m^3 and transported at velocities of 0.1–0.7 m/s. Li et al. (2004) report a value of about 280 kg/m^3 (wet bulk density of about 1,200 kg/m^3) as the transition from the mobile fluid mud to the immobile consolidating bed (about 10 μm) for the mouth of the Yangtze Estuary in China. Consolidation tests of koalinite (about 4 μm) in saline water (van Rijn 1993) show that the consolidation process commences at a concentration of about c_{gel} =150–250 kg/m^3. Dankers (2003) found much lower values of c_{gel}=70–90 kg/m^3 for kaolinite (about 4 μm) in saline water.

Initiation of Motion

Particle movement will occur when the instantaneous fluid force on a particle is just larger than the instantaneous resisting force related to the submerged particle weight and the friction coefficient. The degree of exposure of a grain with respect to the surrounding grains (hiding of smaller particles resting or moving between the larger particles) obviously is an important parameter determining the forces at initiation of motion. Cohesive forces are important when the bed consists of appreciable amounts of clay and silt particles.

The driving forces are strongly related to the local near-bed velocities. In turbulent flow conditions the velocities are fluctuating in space and time. This makes together with the randomness of both particle size, shape, and position that initiation of motion is not merely a deterministic phenomenon but a stochastic process as well (Zanke 2003).

The fluid forces acting on a sediment particle resting on a horizontal bed consist of skin friction forces and pressure forces. The skin friction force acts on the surface of the particles by viscous shear. The pressure force consisting of a drag and a lift force is generated by pressure differences along the surface of the particle. These forces per unit bed surface area can be reformulated in a time-averaged bed-shear stress.

Initiation of motion in steady flow is defined to occur when the dimensionless bed-shear stress (θ) is larger than a threshold value (θ_{cr}). Thus, $\theta > \theta_{cr}$, with $\theta = \tau_{cr,o}/[(\rho_s - \rho_w) g d_{50}]$; $\tau_{cr,o}$=critical bed-shear stress of cohesionless particles, ρ_s=sediment density, ρ_w =fluid density, $s = \rho_s/\rho_w$=relative density, and d_{50}=median sediment diameter.

The θ_{cr} factor depends on the hydraulic conditions near the bed, the particle shape, and the particle position relative to the other particles. The hydraulic conditions near the bed can be expressed by the Reynolds number $R_* = u_* d/\nu$. Thus $\theta_{cr} = F(R_*)$. The viscous effects (υ=kinematic viscosity coefficient) can also be represented by a dimension particle size $D_* = d_{50}[(s-1)g/\upsilon^2]^{1/3}$ (van Rijn 1993, 2007).

Many experiments have been performed to determine the θ_{cr} values as a function of R_* or D_*. The experimental results of Shields (1936) related to a flat bed surface are most widely used to represent the critical conditions for initiation of motion. The Shields curve represents a critical stage at which only a minor part (say 1–10%) of the bed surface is moving (sliding, rolling, and colliding) along the bed. The Shields' curve is not very accurate for fine sand beds. Based on the data of Miller et al. (1977), the critical shear stress can be best represented by

$$\theta_{cr} = 0.115(D_*)^{-0.5} \quad \text{for } D_* < 4 \tag{2a}$$

$$\theta_{cr} = 0.14(D_*)^{-0.64} \quad \text{for } 4 \leq D_* < 10 \tag{2b}$$

Initiation of motion in combined steady and oscillatory flow (wave motion) can also be expressed in terms of the Shields parameters providing that the "wave period-averaged (absolute) bed-shear stress" is used (van Rijn 1993).

Fig. 1 shows the critical bed-shear stress for particle sizes in the ranges of 4–250 μm [based on Eqs. (2)], neglecting cohesive forces. The critical bed-shear stress decreases from 0.183 to 0.025 N/m^2 for particle sizes decreasing from 250 to 4 μm. The two data points in the silt range (8 and 16 μm, see Fig. 1) taken from Zanke (2003) show that this cohesionless behavior is realistic for pure quartz particles. However, natural beds of fine sediments generally show cohesive effects due to the presence of cohesive, binding forces between the particles. For particle size smaller than 62 μm it is herein assumed that the critical bed-shear stress is affected by cohesive particle–particle interaction effects including clay coating effects ($\phi_{cohesive}$), by packing (or bulk density) effects ($\phi_{packing}$), and by biological and organic material effects (ϕ_{bo}). The critical bed-shear stress is tentatively proposed to be represented as

$$\tau_{cr,bed} = \phi_{bo}\phi_{packing}\phi_{cohesive}\tau_{cr,o} \quad \text{for particles} < 62 \text{ μm(clay and silt range)} \tag{3a}$$

$$\tau_{cr,bed} = \phi_{bo}\phi_{cohesive}\tau_{cr,o} \quad \text{for particles} \geq 62 \text{ μm(sand range)} \tag{3b}$$

Natural beds of fine sediment in the range <62 μm may consist of sand, silt, and clay. The clay fraction generally increases for decreasing mean sediment size of the bed. For particles smaller than 62 μm the cohesive effects will gradually increase and the packing effects will gradually decrease (lower bulk density) for decreasing particle sizes. For sand particles larger than 62 μm the cohesive forces are solely related to the clay fraction (if present), which forms a cohesive coating layer around the sand particles.

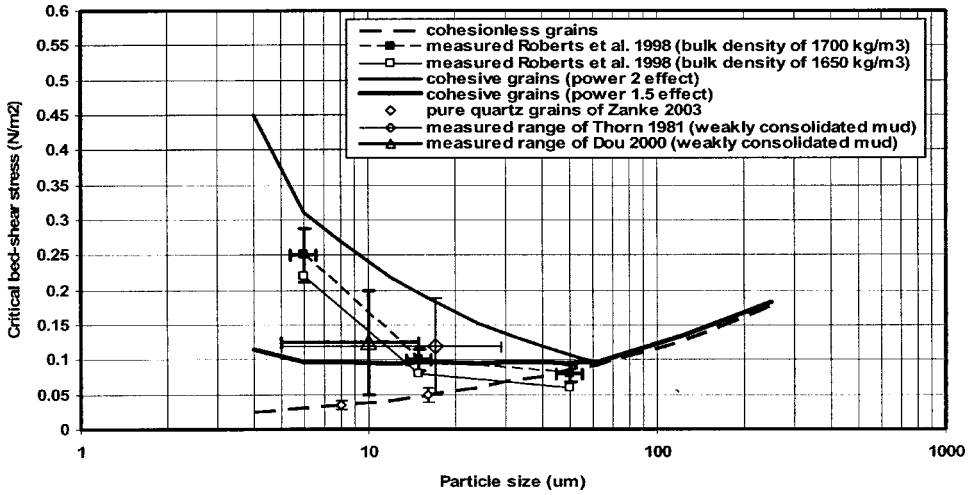

Fig. 1. Effect of cohesive forces on critical bed-shear stress of fine sediment beds (submerged, weakly consolidated beds for particles <62 μm)

Field and laboratory observations of initiation of motion of fine sediment beds (mud–sand beds) have been reported by Delft Hydraulics (1989), van Rijn (1993), Houwing (2000), Dou (2000), and Whitehouse et al. (2000). van Rijn reports critical bed-shear stresses in the range of 0.1–0.3 N/m^2 for weakly consolidated mud beds. Houwing reports values in the range of 0.1–0.5 N/m^2. Dou reports critical depth-averaged velocities (in a flume) in the range of 0.15–0.35 m/s for mud beds (d_{50} in the range of 4–10 μm) with a dry bed density of 200–400 kg/m^3. Assuming a Chézy value of about 80 m$^{0.5}$/s for flat mud beds in a flume, the critical bed shear stress range based on the results of Dou is 0.05–0.2 N/m^2. Thorn (1981) reports similar values for weakly consolidated mud beds (τ_{cr}=0.05–0.19 N/m^2 for sediments in the range of 5–25 μm).

Delft Hydraulics (1989) has determined the critical bed-shear stress of the sand fraction of various natural bed core samples with a diameter of about 0.07 m and lengths up to 2.5 m taken (using vibro-core equipment; May and June, 1989) from a pipeline site in the Dutch Sector of the North Sea. The samples can be roughly classified as: fine sand (100–300 μm), silty sand, and clayey silt, silty clay. The percentages of clay and very fine silt (<8 μm) were estimated to be in the range of 0–50%. The core samples were split in subsamples with a length of about 0.1 m, which were placed in a cylindrical container at the bottom of a laboratory flume. The surface of the sample was exposed to the flow in the flume, which was successively raised until erosion of the bed surface was observed (movement of the sand particles). The critical bed-shear stress for a pure sand sample (200 μm) was found to be about 0.2–0.4 N/m^2, which is somewhat larger than the Shields value of 0.2 N/m^2 for sand with d_{50} of 200 μm. The critical bed-shear stress was estimated from measured critical velocities assuming a logarithmic velocity profile. The samples with $p_{cs}>0.3$ (p_{cs}=proportion of clay in bed sample) show a cohesive behavior with relatively large critical bed-shear stresses ($\tau_{b,cr,sample}/\tau_{b,cr,pure\ sand}>2$). The sandy samples (about 200 μm) show a noncohesive behavior with relatively small critical bed-shear stresses ($\tau_{b,cr,sample}/\tau_{b,cr,pure\ sand}<2$). The results for sand particles (>62 μm) can be roughly represented as

$$\tau_{cr,bed} = (1 + p_{cs})^3 \tau_{cr,o} \tag{3c}$$

Experiments on initiation of motion of cohesive beds consisting of very small quartz particles (<62 μm) with relatively high wet bulk densities (1,600–1,900 kg/m^3) have been done by Roberts et al. (1998). Natural sediment beds consisting of sand, silt and clay (and organic material) have much lower densities, particularly when organic materials are involved (1,100–1,300 kg/m^3; Li et al. 2004). Based on the results of Roberts et al., it can be concluded that the critical bed-shear stress is minimum for about 62 μm (Fig. 1). Cohesive effects become important for particles finer than 62 μm, which is manifest from the increase of the critical bed-shear stress for decreasing particle size. Experimental results of Roberts et al. for particle (quartz) sizes of 6, 15, and 50 μm in a bed with bulk density of about 1,650 and 1,700 kg/m^3 are shown in Fig. 1 with critical bed shear stresses increasing from 0.08 to 0.25 N/m^2 for particle sizes decreasing from 50 to 6 μm. Their experiments also show that the critical bed-shear stress is affected by the packing of the bed (bulk density) and by the presence of clay particles. The presence of 2% Bentonite in a sand bed of relatively high wet density (1,900–2,000 kg/m^3) results in an increase of the critical bed-shear stress by a factor of about 1.5. The representative particle size of fine sediment beds smaller than about 32 μm is not well defined because most of the particles will not be eroded as single particles. Roberts et al. (1998) report that the silt particles (<32 μm) are eroded as aggregates (or chunks; mass erosion) which disintegrate as they are transported downstream.

The cohesive force effects between fine particles are extensively discussed by Lick et al. (2004). Using analysis results of an atomic force microscope, they assume that the cohesive force between two spherical particles can be represented by the particle diameter to the power 2. The binding effects due to the coating of the quartz particles by the clay particles (if present) are similarly related to the particle diameter to the power 2. Herein, it is assumed that both effects can be represented by $\phi_{cohesive}=(d_{sand}/d_{50})^{\gamma}$ with γ in the range of 1–2, d_{sand}=62 μm ($\phi_{cohesive}=1$ for $d_{50}\geq 62$ μm). The packing effects are herein represented as $\phi_{packing}=c_{gel}/c_{gel,s}$ with c_{gel}=gelling volume concentration of the bed (gelling refers to an immobile bed or viscoplastic bed) and $c_{gel,s}$=maximum volume concentration of a pure sand bed ($=1-\eta=0.65$ with η=porosity=0.35); $\phi_{packing}=1$ for $d_{50}\geq 62$ μm. The bed concentration of a natural bed consisting of fine sediments is strongly dependent on the sediment size, the content of organic materials, and the degree of consolidation. A weakly consolidated, submerged mud bed (mixture of clay, silt, and sand) with a mean sediment size <10 μm has a surface bulk (dry) density of about 150–300 kg/m^3. Herein, it is assumed that

$c_{gel}=(d_{50}/d_{sand})c_{gel,s}$ with $c_{min}=0.05$ ($\cong 130$ kg/m^3) for $d_{50}<62$ μm. This yields a gelling concentration varying between about 130 kg/m^3 for $d_{50}=4$ μm and 1,722 kg/m^3 for a pure sand bed with $d_{50}=62$ μm.

The binding effect of the clay fraction in a bed of sand (≥ 62 μm) is caused by coating of the surface of the quartz particles by a layer of clay particles. This latter effect can be represented as $\phi_{cohesive}=\phi_{cs}=(1+p_{cs})^3$ with p_{clay}=proportion of clay fraction (<8 μm) in the bed for $d_{50}\geq 62$ μm (van Rijn 2005); $\phi_{cs}=1$ for $p_{cs}=0$. The presence of organic material may also have a great effect on the erosional behavior of a mud bed. Furthermore, the bed surface may become cemented due to slimes produced by diatoms and bacteria. Herein the biological and organic material factor is assumed to be absent ($\phi_{bo}=1$). At the present stage of research these effects can only be represented by an additional calibration factor. Summarizing, the critical bed-shear stress of a fine sediment bed is proposed to be

$$\tau_{cr,bed}=(c_{gel}/c_{gel,s})(d_{sand}/d_{50})^{\gamma}\tau_{cr,o} \quad \text{for particles} < 62\ \mu\text{m (clay and silt range)} \tag{4a}$$

$$\tau_{cr,bed}=(1+p_{cs})^3\tau_{cr,o} \quad \text{for particles} \geq 62\ \mu\text{m (sand range)} \tag{4b}$$

Eq. (4*a*) is shown in Fig. 1 for $\gamma=2$ and 1.5. The best agreement with the experimental results of Thorn (1981) and Dou (2000) are obtained for a power of $\gamma=1.5$. This latter value is herein used. The critical bed-shear stress according to Eq. (4*a*) is found to be an approximately constant value of 0.1 N/m^2 for a (weakly consolidated) fine sediment bed with sizes in the range of 8–62 μm. The maximum ratio of τ_{cr} and $\tau_{cr,o}$ is on the order of 3–4 for sediments smaller than about 10 μm (see Fig. 1). Using $\tau_{cr}=0.1$ N/m^2 and $C=100$ m$^{0.5}$/s (for field conditions) results in a critical depth-averaged current velocity of about 0.32 m/s. Using $\tau_{cr}=0.2$ N/m^2 and $C=100$ m$^{0.5}$/s results in a critical depth-averaged current velocity of about 0.42 m/s for sediment beds with $d_{50}<62$ μm. These values are quite realistic for fine sediment beds in estuaries.

Bed Forms and Bed Roughness

One of the basic problems in the prediction of sediment transport is the prediction of bed roughness, because sediment transport is strongly dependent on bed roughness, whereas the bed roughness in turn depends on the sediment transport generated by the bed forms migrating over the bed.

Therefore, first the problem of bed roughness prediction is addressed. Since a generally accepted method for the accurate prediction of bed form dimensions in combined steady and oscillatory flow is not yet available, it is proposed to relate the bed roughness (k_s) directly to hydrodynamic and sediment-dynamic parameters (k_s/d_{50}=function(ψ) with d_{50}=median bed diameter and $\psi=U_{wc}^2/[(s-1)gd_{50}]$=dimensionless mobility parameter, U_{wc}=velocity parameter for combined wave-current conditions [see Eq. (5) for general definition]. Dimensional analysis shows that particle size, particle mobility, and grain-related Reynolds number are the most basic parameters influencing bed roughness (Yalin 1977). Assuming hydraulically rough flow conditions, the Reynolds number effect is herein neglected. A brief overview of the types of bed forms involved in hydraulic roughness is given below. A detailed summary is given by van Rijn and Walstra (2003).

The bed form regimes for steady flow over a sand bed can be roughly classified into: (1) lower transport regime with flat bed, ripples, dunes, and bars; (2) transitional regime with washed-out dunes and sand waves; and (3) upper transport regime (Froude number $F>0.8$ and Shield number $\theta>1$) with flat mobile bed and anti-dunes; sand waves may occur in the upper regime with $F<0.8$ and $\theta>1$.

When the velocities are somewhat larger (10–20%) than the critical velocity for initiation of motion and the median particle size is smaller than about 500 μm, small ripples are generated at the bed surface. Ripples generally remain small with a ripple length much smaller than the water depth. The characteristics of ripples are commonly assumed to be related to the turbulence characteristics near the bed (burst–sweep cycle). Current ripples have an asymmetric profile with a relatively steep downstream face (lee side) and a relatively gentle upstream face (stoss side). As the velocities near the bed become larger, the ripples become more irregular in shape, height and spacing yielding strongly three-dimensional ripples. In that case the variance of the ripple length and height becomes rather large. These ripples are called lunate ripples when the ripple front has a concave shape in the current direction (crest is moving slower than wing tips) and are called linguoid ripples when the ripple front has a convex shape (crest is moving faster than wing tips). The largest ripples may have a length up to the water depth and are herein defined as megaripples. Another typical bed form type of the lower regime is the dune-type bed form with a length scale much larger than that of the megaripples. Dunes have an asymmetric (triangular) profile with a rather steep lee side and a gentle stoss side. A general feature of dune type bed forms is lee-side flow separation resulting in strong eddy motions downstream of the dune crest. The length of the dunes is strongly related to the water depth (h) with values in the range of 3–15 h. Extremely large dunes with heights of the order of 7 m and lengths of the order of 500 m have been observed in the Parana River, Argentina, at water depths of about 25 m, velocities of about 2 m/s, and bed material sizes of about 300 μm. Dune type bed forms generally are absent when the sediment bed is finer than about 100 μm. In these latter conditions the bed generally consists of a flat mobile surface and or of large-scale sand waves with a smooth surface with or without small-scale ripples superimposed.

It is a well-known phenomenon that the bed forms generated at low velocities are washed out at high velocities. It is not clear, however, whether the disappearance of the bed forms is accomplished by a decrease of the bed form height, by an increase of the bed form length, or both. Flume experiments with sediment material of about 450 μm showed that the transition from the lower to the upper regime was effected by an increase of the bed form length and a simultaneous decrease of the bed form height (van Rijn 1993). Ultimately, relatively long and smooth sand waves with a roughness equal to the grain roughness were generated in subcritical flow conditions in the flume (van Rijn 1993). Large-scale sand waves with a relative height (Δ/h) of 0.1–0.2 and a relative length (λ/h) of 5–15 were present in the Mississippi River at high velocities in the subcritical upper regime. These sand waves should be considered as relicts of dunes, still in a process of washing away. In the upper regime with $F>0.8$ the bed form types will be plane bed standing waves or anti-dunes.

Bed Forms in Tidal Estuaries

The bed forms most frequently observed in tidal flow are asymmetric megaripples and weakly asymmetric or symmetric sand

waves. Megaripples have a height of 0.03–0.1 times the water depth and a length scale of the order of the water depth. Generally, they are generated in the flood and ebb channels with bed material sizes smaller than about 500 μm. The shape of the megaripples is typical asymmetric in the direction of the main current. Reorientation takes place with reversal of the tide. Sand waves generally have lengths of several times (10–20) the water depth and heights of the order of 0.1 times the water depth. Sand waves are generated in tidal channels with relatively fine sediment beds (<150 μm), as observed in the Changjiang Estuary near Shanghai, China (Li et al. 1993). The bed roughness of sand waves is approximately equal to that of a sheet-flow plane bed (mostly grain/sheet flow roughness).

Bed Forms in Coastal Seas

The dominant bed forms in oscillatory flow (surface waves) with or without a weak current in field conditions often are ripples with a length scale related (smaller or equal) to the near-bed orbital diameter. The ripples are sometimes irregular or have three-dimensional patterns, but are more commonly approximately two dimensional. Ripples exhibiting the formation of fluid vortices (orbital excursion larger than ripple length) are called vortex ripples (Bagnold 1946). Field studies have shown that besides vortex ripples there is a variety of other bed form types and patterns. The variability in bed form morphology is the result of the complex combination of currents and unsteady shoaled waves of many frequencies and directions. Analysis of field data shows the presence of short wave ripples (SWRs) and long wave ripples (LWRs) as the dominant bed forms in conditions with combined waves and weak currents. The bed forms in coastal conditions (ripples) reach a maximum height and length, which are dependent on the particle size (d_{50}), wave period (T_p), and peak near-bed orbital velocity (U_w). Based on the analysis of many data sets (Vongvisessomjai 1984; Kos'yan 1988; Nielsen 1992; van Rijn 1993; van Rijn et al. 1993, 2005; Mogridge et al. 1994; Wiberg and Harris 1994; Slaattelid and Myrhaug 1994; van Rijn and Havinga 1995; Li and Amos 1998; Hanes et al. 2001; Doucette 2002; Grasmeijer and Kleinhans 2004; Traykovski and Goff 2003), SWR are found to be dominant for $\psi=(U_w)^2/[(s-1)gd_{50}$; U_w=peak orbital velocity] in the range of 50–150 and disappear for $\psi>150$. The bed-form height is in the range of 100 to $1{,}000d_{50}$; the bed-form length is in the range of $1{,}000-10{,}000d_{50}$. SWR reformation can occur within 1 min or so after flattening, when the ψ value decrease to a value below 150 but larger than about 50. For $\psi<50$ ripple movement is slow. LWRs are low-relief bed features (steepness of about 0.01) and are always present on the bed surface, but are dominantly present for $\psi>150$. LWRs have a height of 0.01–0.02 m and a length of 1–2 m in a fine sand bed (100–300 μm). The origin of the LWR is not quite clear (Hanes et al. 2001).

Bed Roughness Predictor

Nikuradse (1932) introduced the concept of an equivalent or effective sand roughness height (k_s) to simulate the hydraulic roughness of arbitrary roughness elements of the bottom boundary. In case of a movable bed consisting of sediments the effective bed roughness (k_s) consists of grain roughness (k_s') generated by skin friction forces and of form roughness (k_s''), generated by pressure forces acting on the bed forms. Similarly, a grain-related bed-shear stress (τ_b') and a form-related bed-shear stress (τ_b'') can be defined. The effective bed roughness for a given bed material size is not constant but depends on the flow conditions. Analysis results of k_s values computed from Mississippi River data (United States) show that the k_s value strongly decreases from about 0.5 m at low velocities (0.5 m/s) to about 0.001 m at high velocities (2 m/s), probably because the bed forms become more rounded or are washed out at high velocities (see Fig. 4).

Four types of bed-roughness values can be distinguished (see van Rijn 1993; van Rijn and Walstra 2003): grain roughness ($k_{s,\text{grain}}$); wave-related bed form roughness ($k_{s,w}$); current-related bed form roughness ($k_{s,c}$); and apparent bed-roughness (k_a). Many papers have been written on this topic (see van Rijn 2006). The new prediction method is the parameterization of the results of these works. The definitions and the significance of these four types of roughness contributions are described below.

Current-Related Bed Roughness ($k_{s,c}$)

The physical current-related bed roughness value ($k_{s,c}$) of bed forms is the roughness experienced by the current in condition with and without waves. The effective bed roughness of ripple type and dune type bed forms in rivers (no waves) are in the range of 0.1–1.5 times the bed form height (van Rijn 1984a,b,c). Analysis of velocity profiles measured above a fine-sand bed (100 μm) with ripples generated in a wave-current basin shows k_s values in the range of 0.1–1.5 times the ripple height (or $k_s/\Delta_r=0.1-1.5$ with a mean value of 0.75) (Fredsøe et al. 1999; Havinga 1992; and van Rijn and Havinga 1995).

Fredsøe et al. (1999) have studied the effective roughness of artificial ripples (concrete ripples) based on measured velocity profiles in a wave-current flume. The bed of the flume was covered with sharp-crested wave-type ripples (length of 0.22 m and height of 0.035 m) made of concrete. Three types of experiments were carried out: current alone, waves alone, and combined waves current. The k_s values were determined by regression analysis of velocity profiles from the current-alone experiments resulting in k_s values in the range of 2.1–2.3 times the ripple height ($k_s/\Delta_r=2.1-2.3$).

Herein, it is assumed that the physical bed roughness of movable ripples (SWR) in natural conditions is approximately equal to the ripple height: $k_{s,c}=\Delta_r$ (van Rijn and Havinga 1995). Furthermore, it is assumed that ripples (SWR) are fully developed with a height equal to $\Delta_r=150d_{50}$ for $\psi\leqslant 50$ in the lower wave-current regime and that the ripples (SWR) disappear with $\Delta_r=0$ for $\psi\geqslant 250$ in the upper wave-current regime (sheet flow conditions) (van Rijn and Walstra 2003). In the former case the bed roughness is fully determined by form roughness, while in the latter case the physical roughness is fully determined by the moving grains in the sheet flow layer (Bayram et al. 2003; Wilson 1989; Sumer et al. 1996). LWR may be present in the upper regime, but the form roughness of LWR is assumed to be zero (no vortex generation). Based on all available information, it is proposed that the physical current-related roughness of small-scale ripples is given by

Ripples

$$k_{s,c,r}=150f_{cs}d_{50} \quad \text{for } \psi\leqslant 50$$

(lower wave-current regime, SWR ripples) (5*a*)

$$k_{s,c,r}=20f_{cs}d_{50} \quad \text{for } \psi>250$$

(upper wave-current regime; sheet flow) (5*b*)

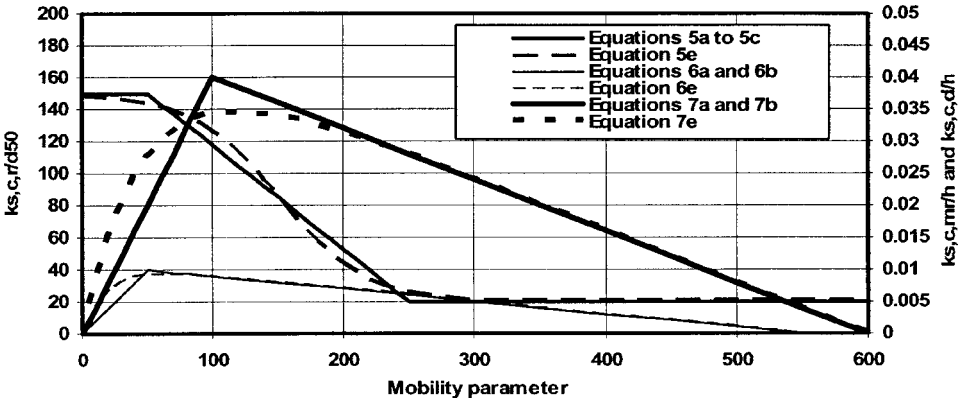

Fig. 2. Current-related roughness of ripples, megaripples, and dunes for sand range

$$k_{s,c,r} = (182.5 - 0.652\psi) f_{cs} d_{50} \quad \text{for } 50 < \psi \leq 250$$

(transitional regime; linear approach) (5*c*)

$$k_{s,c,r} = 20 d_{silt} \quad \text{for } d_{50} < d_{silt} \tag{5d}$$

where ψ=current-wave mobility parameter=$U_{wc}^2/[(s-1)gd_{50}]$, $(U_{wc})^2=(U_w)^2+u_c^2$; s=relative density=ρ_s/ρ_w, U_w=peak orbital velocity near bed=$\pi H_s/[T_r \sinh(2kh)]$, u_c=depth-averaged current velocity, H_s=significant wave height; $k=2\pi/L$; L=wave length derived from $(L/T_p \pm u_c)^2=gL \tanh(2\pi h/L)/(2\pi)$; T_r=relative wave period; T_p=peak wave period; h=water depth; $f_{cs}=(0.25d_{gravel}/d_{50})^{1.5}$; $f_{cs}=1$ for $d_{50} \leq 0.25 d_{gravel}$; and d_{gravel}=0.002 m. The f_{cs} factor which expresses the effect of a gradually decreasing ripple roughness for very coarse sediment beds (>500 μm), is a best guess expression in the absence of coarse bed data. It can be modified when field data become available.

Eqs. (5*a*)–(5*d*) include the grain roughness and is assumed to be valid for sediment with d_{50} in the range of about 10–2,000 μm. The maximum bed roughness is of the order of 0.075 m for sand with d_{50}=500 μm. The lower limit is $k_{s,c}=20d_{silt}$=640 μm for particles ≤32 μm. Eqs. (5*a*)–(5*c*) based on three linear expressions, can also be expressed by a smooth curve over the full ψ range, as follows

$$k_{s,c,r} = f_{cs} d_{50} \{85 - 65 \tanh[0.015(\psi - 150)]\} \tag{5e}$$

Fig. 2 shows Eqs. (5*a*)–(5*c*) and Eq. (5*e*) as a function of dimensionless variables for the sand range. Fig. 3 shows the current-related ripple roughness ($k_{s,c,r}$) as a function of the depth-averaged velocity (u) and the particle size of the bed (from 8 to 2000 μm) based on Eqs. (5*a*)–(5*d*). The ripple roughness values range from 0.00064 to 0.075 m; the values are largest for small velocities and decrease for increasing velocities.

Besides SWR, often megaripples with a length scale of the water depth and/or dunes with a length scale much larger than the water depth are present on the seabed (if h=water depth>1 m). Due to the difference in their length scales the roughness values of megaripples and dunes are represented herein as separate values. Megaripples and dunes are assumed to be absent for silt and clay beds. van Rijn (1984c, 1993) has shown that megaripples and dunes are related to the flow depth (h) and to the flow regime (mobility parameter). The bed-form height first increases and then decreases for increasing mobility. The physical bed form roughness ($k_{s,c,mr}$) of the megaripples and dunes ($k_{s,c,d}$) is roughly on the order of half the bed form height (van Rijn 1984c, 1993). Herein, the bed form dimensions are not described explicitly, but it is proposed to use a direct parameterization of the effective bed roughness. Based on the available information, the bed roughness of megaripples is expressed as a function of the flow depth (h) and the mobility parameter (ψ) (see Fig. 2)

Mega-ripples

$$k_{s,c,mr} = 0.0002 f_{fs} \psi h \quad \text{for } \psi \leq 50 \tag{6a}$$

$$k_{s,c,mr} = (0.011 - 0.00002\psi) f_{fs} h \quad \text{for } 50 < \psi \leq 550 \tag{6b}$$

$$k_{s,c,mr} = 0.02 \quad \text{for } \psi > 550 \text{ and } d_{50} \geq 1.5\, d_{sand} \tag{6c}$$

$$k_{s,c,mr} = 200 d_{50} \quad \text{for } \psi > 550 \text{ and } d_{50} < 1.5\, d_{sand} \tag{6d}$$

$$k_{s,c,mr} = 0 \quad \text{for } d_{50} < d_{silt}$$

with $f_{fs}=(d_{50}/1.5d_{sand})$; $f_{fs}=1$ for $d_{50} \geq 1.5 d_{sand}$; d_{sand}=0.000062 m. Eq. (6*c*) specifies that the lower limit is k_s=0.02 m for practice (some undulations will always be present on the bed). The f_{fs} factor, which expresses the effect of a gradually decreasing megaripple roughness for very fine sediment beds, is a best guess parameter in the absence of data. It can be improved when field data become available.

Eqs. (6*a*)–(6*d*) yield: $k_{s,c,mr}=0.01h$ for ψ=50 and $k_{s,c,mr}$=0.02 m for ψ=250, see Fig. 2. Hence, the maximum value is $k_{s,c,mr}=0.01h$ (with an absolute maximum value set to 0.2 m) and the minimum value is either 0.02 m for d_{50}>100 μm or $200d_{50}$ for fine sediment <100 μm. The megaripple roughness values are up to 0.1 m (Fig. 3). The minimum bed roughness in the upper regime of a sand bed (>100 μm) is assumed to be k_s=0.02 m, expressing the effect that a sand bed in the upper regime is never completely flat but vague undulating features often remain present along the bed.

Eqs. (6*a*) and (6*b*) based on two linear expressions can also be represented by a smooth curve (see also Fig. 2), as follows

$$k_{s,c,mr} = 0.00002 f_{fs} h [1 - \exp(-0.05\psi)](550 - \psi) \tag{6e}$$

Similar to the roughness of megaripples, the effective roughness of dunes is proposed to be described by a direct parameterization based on the flow depth and the mobility parameter, as follows (see Fig. 2)

Dunes

$$k_{s,c,d} = 0.0004 f_{fs} \psi h \quad \text{for } \psi \leq 100 \tag{7a}$$

$$k_{s,c,d} = (0.048 - 0.00008\psi) f_{fs} h \quad \text{for } 100 < \psi \leq 600 \tag{7b}$$

$$k_{s,c,d} = 0 \quad \text{for } \psi > 600 \tag{7c}$$

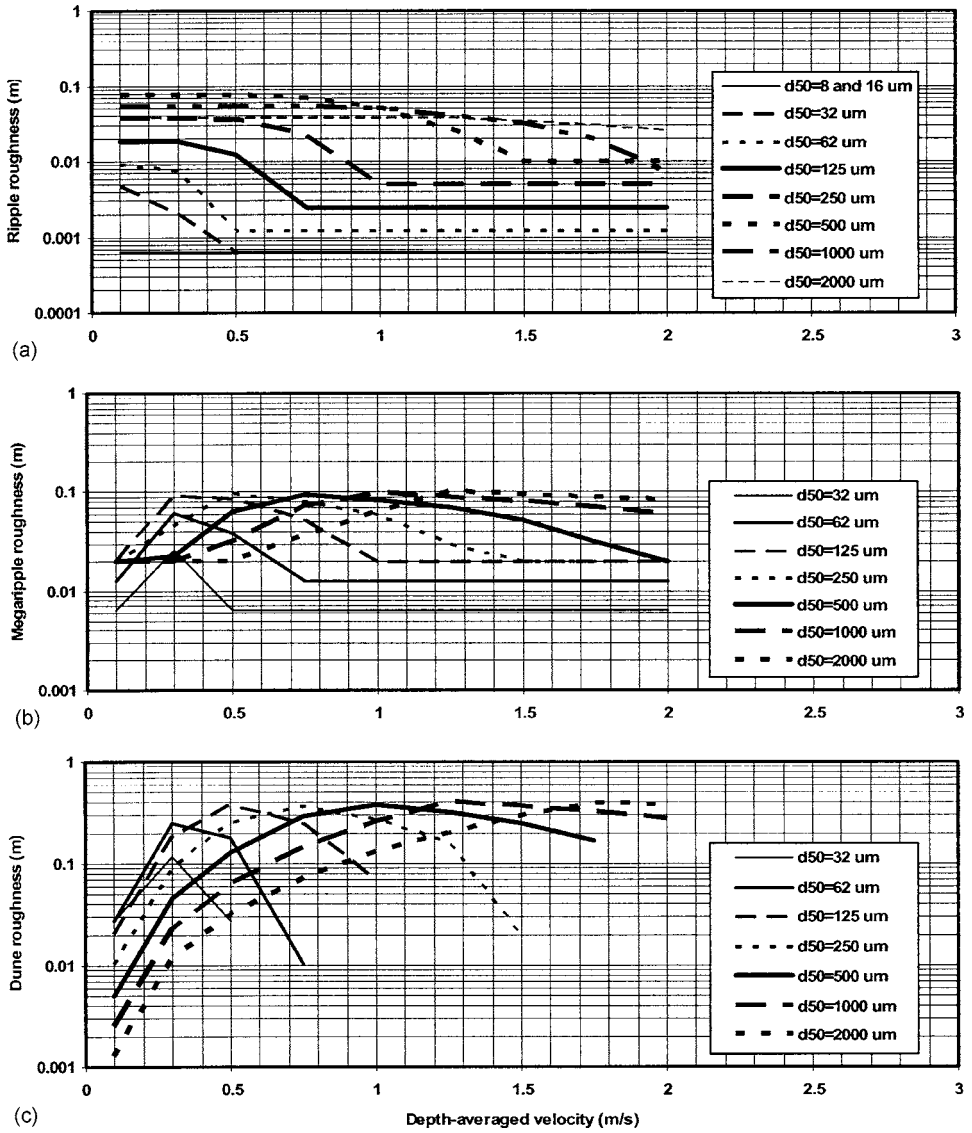

Fig. 3. Current-related roughness of ripples (a); megaripples (b); and dunes (c) as function of depth-averaged velocity for sediment of 8–2000 μm (h=10 m)

$$k_{s,c,d} = 0 \quad \text{for } d_{50} < d_{\text{silt}} \tag{7d}$$

Eqs. (7*a*)–(7*d*) yield: $k_{s,c,d}$=0 for ψ=0, $k_{s,c,d}$=0.04h for ψ=100, and $k_{s,c,d}$=0 for ψ=600, see Fig. 2. Hence, the maximum value is $k_{s,c,d}$=0.04h (with an absolute maximum set to 1 m). The roughness values of dunes are up to 0.4 m for sand up to 2,000 μm (see Fig. 3).

Eqs. (7*a*) and (7*b*) based on two linear expressions can also be represented by a smooth curve (see also Fig. 2), as follows

$$k_{s,c,\text{mr}} = 0.00008 f_{\text{fs}} h[1 - \exp(-0.02\psi)](600 - \psi) \tag{7e}$$

Roughness values based on Eqs. (5)–(7) are shown in Fig. 3 for a water depth of 10 m, Te=15°C, and Sa=30 promille. The roughness of ripple and megaripples varies approximately are up to 0.075 and 0.1 m, respectively. Dunes have roughness values up to 0.4 m for sand in the range of 500–2000 μm. The roughness of megaripples and dunes is relatively small for low velocities, increases as the current velocity increases, and then decreases again for the largest velocities in the upper regime (washed out bed forms). The ripples show a similar behavior, but relict ripple roughness is assumed to be present at low velocities.

The small-scale ripples may be superimposed on megaripples and/or large-scale dunes at specific locations. The effective roughness of the (symmetric) sand waves is approximately zero, because flow separation does not occur. These large-scale sand waves can be seen as topography for the flow system.

When megaripples and/or dunes are present, these values are herein added to the physical bed roughness of the small-scale ripples by quadratic summation. Thus, the total physical current-related roughness ($k_{s,c}$) is based on

$$k_{s,c} = [(k_{s,c,r})^2 + (k_{s,c,\text{mr}})^2 + (k_{s,c,d})^2]^{0.5} \tag{8}$$

The current-related friction coefficient (based on the Darcy–Weisbach approach: $f=8g/C^2$) can be computed as: $f_c = 8g/[(18\log(12h/k_{s,c})\,]^2$. It is realized that Eq. (8) is not correct from a pure physical point of view, because basically the friction factors should be added. The expressions (5)–(8) are partly intuitive, engineering expressions rather than exact theoretical formulations. This latter approach is beyond the existing knowledge of two-phase flow over a dynamic, mobile bed. The proposed expressions produce, however, values of the right order of magni-

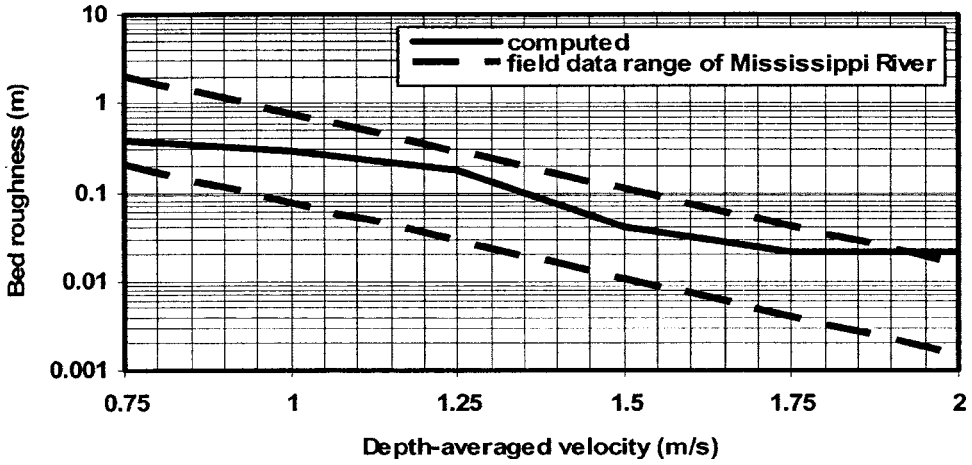

Fig. 4. Bed roughness as function of depth-averaged velocity for Mississippi River (h=10 m, d_{50}=250 μm)

tude. Fig. 4 shows measured and computed bed roughness values for the Mississippi River (United States) over a velocity range of 0.75–2 m/s. The measured data (depths of 5–15 m; d_{50} of 150–300 μm) are taken from the compendium of Peterson and Howells (1973) (see Fig. 6.1.1. of van Rijn 1993). The computed values based on Eqs. (5)–(8) are of the right order of magnitude and lie within the field data range. The reduction of the bed roughness in the upper flow regime can be clearly observed, but the minimum value of about 0.02 m [Eq. (6)] in the upper regime may be somewhat too high. The proposed method will be tested more severely as an integral part of the sediment transport model (Part 2).

Wave-Related Roughness of Movable Bed $k_{s,w}$

The physical wave-related bed form roughness value ($k_{s,w}$) of wave-induced ripples can be derived from analysis of measured instantaneous velocity profiles within the wave boundary layer or from the attenuation of measured wave heights over a certain distance. The $k_{s,w}$ parameter is strongly related to flow separation and vortex shedding due to oscillatory flow (wave motion) over ripples. Data analysis (van Rijn 1993) shows values in the range of 1–3 times the ripple height ($k_{s,w}/\Delta_r$=1–3). With regard to the physical wave-related bed roughness, only bed forms (ripples) with a length scale on the order of the wave orbital diameter near the bed are relevant. Bed forms (megaripples, ridges, sand waves) with a length scale much larger than the orbital diameter do not contribute to the wave-related roughness. Herein, it is assumed that the physical wave-related roughness of movable small-scale ripples (SWR) in natural conditions is approximately equal to the ripple height: $k_{s,w}=\Delta_r$ (van Rijn and Havinga 1995). Furthermore, it is assumed that ripples (SWR) are fully developed with a height equal to $\Delta_r=150d_{50}$ for $\psi \leqslant 50$ in the lower wave-current regime and that the ripples (SWR) disappear with $\Delta_r=0$ for $\psi \geqslant 250$ in the upper wave-current regime (sheet flow conditions) (van Rijn and Walstra 2003). In the former case the bed roughness is fully determined by form roughness, while in the latter case the physical roughness is fully determined by the moving grains in the sheet flow layer and the bed roughness is in the order of the wave boundary layer thickness (Bayram et al. 2003; Wilson 1989; Sumer et al. 1996). LWR may be present in the upper regime, but the form roughness of LWR is assumed to be zero (no vortex generation). All these effects are taken into account by the new roughness prediction method. Similar to the current-related ripple roughness, it is proposed that the physical wave-related roughness of small-scale ripples is given by Eqs. (5*a*)–(5*d*). Thus: $k_{s,w,r}=k_{s,c,r}$.

The wave-related friction coefficient can be computed as: $f_w=\exp[-6+5.2(A_w/k_{s,w,r})^{-0.19}]$ with A_w=peak orbital diameter near the bed.

Apparent Bed Roughness (k_a)

In steady flow superimposed by surface waves the apparent bed roughness (k_a) is the dominant roughness factor due to wave–current interaction processes. The apparent bed roughness parameter can be derived from measured velocity profiles in the presence of waves over a rippled bed surface using the velocity data outside the wave boundary layer (see Fredsøe et al. 1999).

The apparent roughness (k_a) can be much larger than the physical roughness ($k_{s,c}$) depending on the relative strength of the peak orbital velocity (U_w) and the depth-averaged current velocity (u_c) and the angle between the wave direction and the current direction. Based on analysis of laboratory data (sand ripples in movable-bed experiments) in a wave-current basin (van Rijn 1993), the following empirical expression was proposed (see also Nielsen 1992; You and Nielsen 1996)

$$k_a/k_{s,c}=\exp(\gamma U_w/u_c) \quad \text{with maximum value of 10} \qquad (9)$$

where $\gamma=0.8+\varphi-0.3\varphi^2$ and φ=angle between wave direction and current direction (in radians between 0 and π; $\varphi=0.5\pi=90°$, $\varphi=\pi=180°$). Characteristic γ value are $\gamma=0.8$, for $\varphi=0$; $\gamma=1$ for $\varphi=\pi=180°$; and $\gamma=1.63$ for $\varphi=0.5\pi=90°$. The γ value is maximum $\gamma=1.63$ for $\varphi=0.5\pi=90°$.

Fredsøe et al. (1999) have summarized the k_a values for artificial ripples in laboratory flumes and basins (nine data sets). Most values of the k_a/k_s ratio are in the range of 1 and 15 depending on the relative strength of the wave and current motion, the wave height and the wave direction. Eq. (9) was applied by Fredsøe et al. to their experimental values with good results.

Garcez Faria et al. (1998) have analyzed a large data set from the Duck94 experiment (United States). Velocity profiles of the longshore current were measured in the surf zone of the Duck beach site (sand of 150–200 μm). Water depths are in the range of 1.5–4 m; depth-mean current velocities are in the range of 0.2–1 m/s, and significant wave heights are in the range of 0.8–1.8 m. Bed irregularities (k_r) were measured with a 1 MHz

sonic altimeter mounted on the CRAB (11 m high, motorized, three wheel vehicle) at 0.7 m from the bed and presented as rms-values in the range of 0.0005–0.11 m. The k_a values were determined from the z intercept ($z_a=k_a/30$) of the linear regression on a semilog-plot of z versus velocity $u(z)$, resulting in k_a values in the range of 0.001–2 m. Based on a data set of 19 values, the ratio k_a/k_r varies in the range of 0.3–50, with a mean value of about 11. The ratio of U_w and u_c varies in the range of 0.9–5.4, with a mean value of 1.9. Thus, $k_a/k_r \cong 11$ for $U_w/u_c \cong 1.9$ and $\varphi \cong 90°$. The data do not show a clear correlation between k_a/k_r and U_w/u_c. Eq. (9) yields a value of $k_s/k_{s,c}=10$ for these conditions.

Johnson (2004) performed a series of experiments related to the bed-shear stress over a rippled bed in the case of a longshore current in a large-scale wave-current basin. The bed-shear stresses along the nearshore profile were measured to be in the range of 0.15–0.25 N/m^2 for water depths in the range of 0.15–0.25 m and depth-averaged velocities in the range of 0.08–0.1 m/s. The significant wave height is about 0.15 m (period of about 2 s). The bed material diameter is about 150 μm. Small-scale wave-induced ripples were observed to be present. The present model yield also has values in the range of 0.15–0.25 N/m^2 in excellent agreement with those of Jonhson (2004).

Houwman and van Rijn (1999) have shown that the apparent roughness is almost constant over a wide range of peak orbital velocities (0.3–1.5 m/s). This behavior is caused by the strong decrease of the physical bed roughness for increasing orbital velocity due to the disappearance of the bed ripples (ripples are washed at relatively high orbital velocities in the sheet flow regime), while the amplification effect (ratio $k_a/k_{s,c}$) strongly increases for increasing orbital velocities. A constant apparent bed roughness of 0.1 m was found to give the best agreement between all measured and predicted current velocities (0.3–0.5 m/s at 1.2 m above the bed) at two sites (water depths of 5–10 m, sand of 200 μm; orbital velocities up to 0.6 m/s) near the island of Terschelling in the Dutch sector of the North Sea.

Bed-Load Transport

Usually, the transport of particles by rolling, sliding, and saltating is called the bed-load transport. In the lower regime the bed-load transport is strongly related to the migration of bed forms (ripples and dunes). In the upper regime a thin high-concentration sheet flow layer is present just above the bed, in which the sediment concentrations vary from the maximum value (order of 1,500 kg/m^3) to about 10 kg/m^3 over a thickness of the order of 0.01 m. As this latter type of sediment motion is strongly related to particle–particle interaction and gravity and not so much to turbulence-induced forces (largely damped due to the presence of particles, see Part 2), it is herein defined as bed-load transport. Many formulas to predict the bed-load transport rate in steady flows are described in the literature (see van Rijn 1993 and Soulsby 1997). The first reliable empirical formula was presented by Meyer-Peter and Mueller (1948). They performed flume experiments with uniform particles and with particle mixtures. Based on data analysis, a relatively simple formula was obtained, which is frequently used. Einstein (1950) introduced statistical methods to represent the turbulent behavior of the flow. Einstein gave a detailed but complicated statistical description of the particle motion in which the exchange probability of a particle is related to the hydrodynamic lift force and particle weight. Einstein proposed the d_{35} as the effective diameter for particle mixtures and the d_{65} as the effective diameter for grain roughness. Bagnold (1966) introduced an energy concept and related the sediment transport rate to the work done by the fluid. van Rijn (1984a,b,c) solved the equations of motions of an individual bed-load particle and computed the saltation characteristics and the particle velocity as a function of the flow conditions and the particle diameter for plane bed conditions.

Herein, the attention is focussed on the development of a general bed-load transport equation that can be used for both steady and oscillatory flows. This can be done by using the concept of the instantaneous bed-shear stress. The instantaneous bed-load transport rate ($q_{b,t}$ in kg/s/m) is related to the instantaneous bed-shear stress, which is based on the instantaneous velocity vector (including both wave-related and current-related components; numerical intrawave approach) defined at a small height a (=top of bed load layer) above the bed. Ribberink (1998) has shown that this method works very well for sand larger than about 0.2 mm. Proper predictive modeling of the wave-related (oscillating) transport components basically requires an accurate description of the near-bed orbital fluid velocity, especially in conditions with shoaling and breaking waves (nonlinear wave motion; asymmetric waves). Herein, the method of Isobe–Horikawa (1982) modified by Grasmeijer (2002) is used. The net bed-load transport rate can be obtained by time averaging (over the wave period T) of the instantaneous transport rate using a bed-load transport formula (quasi-steady approach), as follows: $q_b=(1/T)\int(q_{b,t})\mathrm{d}t$. The bed-load transport model for steady flow proposed by van Rijn (1984a, 1993) is a parameterization of a detailed grain saltation model representing the basic forces acting on a bed-load particle. This model is herein slightly modified to better deal with steady flow plus waves, yielding

$$q_b = \gamma \rho_s f_{\mathrm{silt}} d_{50} D_*^{-0.3} (\tau'_{b,cw}/\rho)^{0.5} [(\tau'_{b,cw} - \tau_{b,\mathrm{cr}})/\tau_{b,\mathrm{cr}}]^{\eta} \qquad (10)$$

in which $\tau'_{b,\mathrm{cw}}$=instantaneous grain-related bed-shear stress due to both currents and waves=$0.5\ \rho_w f'_{\mathrm{cw}} (U_{\delta,\mathrm{cw}})^2$, $U_{\delta,\mathrm{cw}}$=instantaneous velocity due to currents and waves at edge of wave boundary layer; f'_{cw}=grain friction coefficient due to currents and waves $=\alpha\beta f'_c + (1\text{-}\alpha) f'_w$, $f'_c = 8g/\{[18\log(12h/k_{s,\mathrm{grain}})]^2\}$=current-related grain friction coefficient based on $k_{s,\mathrm{grain}}=1d_{90}$; $f'_w=\exp[-6+5.2(A_w/k_{s,\mathrm{grain}})^{-0.19}]$=wave-related grain friction coefficient based on $k_{s,\mathrm{grain}}=1d_{90}$; α=coefficient related to relative strength of wave and current motion=$u_c/(u_c+U_w)$; u_c=depth-averaged current velocity; U_w=peak orbital velocity; β=coefficient related to vertical structure of velocity profile (van Rijn 1993); A_w=peak orbital diameter near the bed; h=water depth (m); $\tau_{b,\mathrm{cr}}$=critical bed-shear stress according to Shields; ρ_s=sediment density; ρ_w=fluid density; d_{50}=particle size; $D_*=d_{50}[(s\text{-}1)g/\nu^2]^{1/3}$=dimensionless particle size; s=relative density; ν=kinematic viscosity coefficient; $f_{\mathrm{silt}}=d_{\mathrm{sand}}/d_{50}$=silt factor ($f_{\mathrm{silt}}=1$ for $d_{50}>d_{\mathrm{sand}}$); γ=coefficient=0.5; and η=exponent=1. The γ and η coefficients were recalibrated using measured data sets (>0.2 mm) of the large-scale wave tunnel of Delft Hydraulics (Ribberink 1998; van Rijn 2000). Ribberink (1998) and coworkers performed a series of experiments on bed-load transport under sheet flow conditions in a large-scale wave tunnel. The experiments concern regular symmetric and asymmetric waves (second-order Stokes) with and without a steady current (following and opposing) over a sand bed (almost uniform sand) with particle sizes in the range of 130–970 μm. Eq. (10), which is valid for both steady and oscillatory flow, is slightly different from that of the TR1993 model (van Rijn 1993). Basic input parameters are: water depth, current velocity, significant wave height (H_s), peak wave period (T_p) and angle between wave and

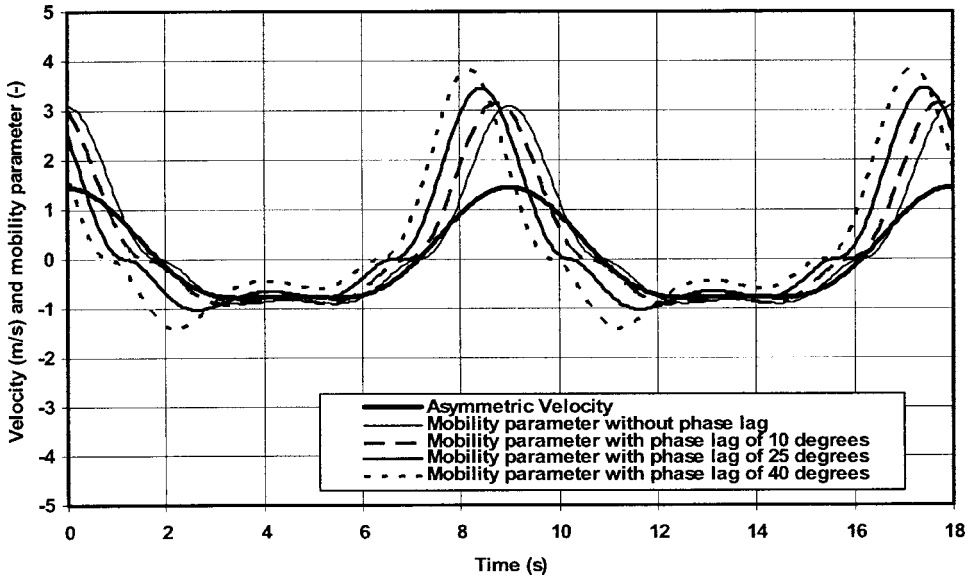

Fig. 5. Velocity and Shields mobility parameter (θ') as function of time; asymmetric velocity signal (U_{max}=1.45 s, U_{min}=0.7 m/s, T=9 s, d_{50}=0.21 mm)

current direction (φ) and sediment characteristics (d_{50} and d_{90}).

Eq. (10) contains two shear stress terms; the second term can be seen as the wave stirring term, whereas the first term is the transport term. This approach is in line with many other bed-load transport formulae (see also Soulsby 1997).

Wave-induced streaming (u_δ) is included based on the work of Davies and Villaret (1997, 1999), who have summarized model and experimental results (see van Rijn and Walstra 2003; van Rijn 2006 for a detailed discussion). Experimental and theoretical studies involving plane rough beds in the turbulent flow regime show that the near-bed streaming depends rather critically upon the bed roughness, as well as on the degree of wave asymmetry. This was already shown by Bijker et al. (1974). The effect of bed roughness is to reduce the phase lead of the bottom velocity in comparison with the 45° lead given by the classical Stokes' solution. This causes the Eulerian streaming to be reduced. Analysis of datasets shows that the wave-induced streaming at the edge of the wave boundary layer is positive or negative (against wave propagation direction) as a function of relative roughness $A_w/k_{s,w}$ with A_w=peak orbital diameter at edge of wave boundary layer and $k_{s,w}$=wave-related bed roughness. The streaming velocity (u_δ) at the edge of wave boundary layer becomes more negative for decreasing relative roughness values ($A_w/k_{s,w}$). The expression involved leads to $u_\delta=0.75(U_w)^2/c$ for $A_w/k_{s,w}\geqslant 100$ (in line with the results of Longuet-Higgins 1953), $u_\delta=-0.125(U_w)^2/c$ for $A_w/k_{s,w}=10$, and $u_\delta=-(U_w)^2/c$ for $A_w/k_{s,w}\leqslant 1$ with c=wave celerity. It is still open for debate whether the results of Davies and Villaret (1999) are sufficiently accurate for the streaming distribution over rippled beds, as the modeling of flow separation phenomena around rippled beds basically requires a two-dimensional horizontal and vertical approach using higher order turbulence closure models (Fredsøe et al. 1999). The streaming velocity at the edge of the wave boundary layer produced by the model of Davies and Villaret certainly is of the right order of magnitude compared with the available laboratory data sets, but the vertical streaming distribution within the boundary layer is not yet severely tested (see Figs. 9–11 from Davies and Villaret 1999). In the present bed-load transport model [Eq. (10)], the streaming velocity is added to the instantaneous orbital velocity at the edge of the wave boundary layer. Hence, wave-induced streaming effects are included.

Madsen (1991) has shown that particle acceleration forces in oscillatory flow can be neglected in the sand range (particles in the range of 0.2–2 mm). This means that the sediment particles react almost instantaneously to the fluid forces. Nielsen (1992, 2002, 2006) and Nielsen and Callaghan (2003) have shown that the fluid accelerations in strongly asymmetric wave motion lead to an increase and phase lead of the bed-shear stresses. Watanabe and Sato (2004) have shown that the fluid acceleration effects on the bed shear stresses lead to a small net transport in the case of forward leaning waves, even if the peak onshore and offshore orbital velocities are equal. Nielsen and Callaghan (2003) have proposed a simple method to deal with these processes, which tentatively (input switch) is included in Eq. (10). Fig. 5 shows the orbital velocity (free-stream velocity) and the grain-related Shields mobility parameter $\{\theta'=\tau'_{b,t'}[(\rho_s-\rho_w)gd_{50}]\}$ within the wave cycle for an experiment of Ribberink et al. (2000) with input data: U_{max}=1.45 m/s, U_{min}=−0.7 m/s, T=9 s, d_{50}=0.21 mm, d_{90}=0.32 mm, $q_{b,net}=108\times10^{-6}$ m^2/s=0.29 kg/s/m. Results with and without acceleration effects (based on method of Nielsen and Callaghan 2003) are shown in Fig. 5. The friction factor used to compute the bed-shear stress is taken as f'_w=0.01. The instantaneous Shields values are shifted forward for phase lags (leads) of 10, 25, and 40°. The peak bed-shear stress increases with increasing phase lag. Using Eq. (10), the net bed-load transport is 0.24 kg/s/m based on a phase lead of 40°, as suggested by Wijetunge and Sleath (1998). This value is close to the measured value of 0.29 kg/s/m. Neglecting the phase effects, the net transport is about 0.13 kg/s/m (about 50% smaller).

As discussed extensively by Ribberink (1998), Dohmen-Janssen (1999), and many others, phase lag effects between shear stress and sediment concentration in the sheet flow layer are extremely important for fine sediments (<0.2 mm). Similar effects do occur above a rippled bed and the net transport (although mainly suspended load transport, see Part 2) may even become negative (against the wave propagation direction), (Dibajnia and Watanabe 1993, 1996, 1998, 2000; van der Werf 2006). It should

be realized, however, that these negative suspended load transport rates have been observed mostly under regular waves and not so much under irregular waves when the ripples generally are much flatter and less steep. Basically, a fully unsteady model is required to deal with these effects. A quasi-steady model [Eq. (10)] cannot accurately represent these effects. However, Dohmen-Janssen (1999) has proposed a method to take phase lags into account. According to Dohmen-Janssen (1999), the phase-lag effects can to some extent be represented by the parameter $p=(\delta_w)/(T\,w_s)$ where δ_w=thickness of wave boundary layer (order of 0.01 m), T=wave period, and w_s=fall velocity. Phase-lag effects are important for fine sediment, large peak orbital velocities, and small wave periods ($p>0.1$). Dohmen-Janssen (1999) suggests that the bed-load transport rate based on a quasi-steady expression should be corrected, using a correction factor (r): $q_{b,\text{net}}=r\ q_{b,\text{net,steady}}$ where r=correction factor between 0 and 1 depending on the p parameter, and $q_{b,\text{net,steady}}$=net bed-load transport given by the quasi-steady expression. This approach is tentatively (input switch) included in Eq. (10). Using this method, the net bed-load transport is gradually reduced for finer sediments. It can however not represent negative transport rates in the rippled bed regime. Neglecting the phase lag effect, Eq. (10) always yields net onshore bed-load transport in asymmetric shoaling waves. The inclusion of phase lags for bed-load transport of fine sediments is not of that great importance, because (1) the bed-load transport is much smaller than the suspended load transport (Part 2) for very fine sediments and (2) beaches consisting of very fine sediments are rare. Finally, it is noted that the effects related to wave asymmetry are dominantly occurring in the nearshore zone close to the beach (swash and inner surf zone). Our knowledge of the sediment transport processes in this latter zone is still very limited and research efforts should be intensified to come up with generally accepted relationships so that we can better deal with beach and dune erosion. The basic problem is that the net transport in this zone is a delicate balance of various onshore and offshore-directed transport processes which are all of the same order of magnitude. Thus, the net result in these conditions is by definition uncertain and almost unpredictable. The present model is far from perfect for the inner surf and swash zone, but it can be used in these conditions as a hindcast model (as shown for two large-scale laboratory cases in Part 4). The model user has to decide which of the processes should be included by using various input switches. Using this approach, a sensitivity study can be done to evaluate which processes are dominant. Sediment transport and associated morphological predictions cannot be done with great accuracy for the complicated inner surf and swash zone, especially not under fair-weather conditions when transport rates are low. However, it is possible to predict ranges of variation over short-term time scale (storm scale) in conditions with dominant suspended load transport, but not on the seasonal time scale (van Rijn et al. 2003) being a combination of low and high wave conditions.

The effect of bed roughness on bed-load transport is mainly through the structure of the near-bed velocity profile, which is herein based on the predicted bed roughness (as explained later). The effect of bed roughness is particularly important for coastal flow (combined steady and oscillatory flow). In the case of steady river flow and quasi-steady tidal flow the bed-load transport is only affected by grain roughness.

The basic parameters influencing the bed-load transport in the silt range of 8–62 μm and in the fine sand range of 62–200 μm are not very well known. In dominantly oscillatory flow the net bed load may become zero or even negative (opposite to the wave propagation direction) due to phase lag effects. Sensitivity computations for the sand range (>200 μm) show that the bed-load transport is only weakly dependent on particle size (see below). The bed-shear stress parameter $[(\tau'_{b,\text{cw}}-\tau_{b,\text{cr}})/\tau_{b,\text{cr}}]$ in the silt range is approximately constant for a given bed-shear stress, because the critical bed-shear stress is approximately constant in the silt range (Fig. 1). Hence, a constant bed-load transport can be obtained by introducing a silt factor ($f_{\text{silt}}=d_{\text{sand}}/d_{50}$). This latter approach will herein be tentatively used for the silt range (<62 μm) in the absence of field data. The precise value of the silt factor is to be determined later by future research, when field data sets become available. Based on the results of various sensitivity computations, it is noted that the bed-load transport generally is much smaller than the suspended load transport in the silt range (<1%) and thus of less importance.

Verification for River and Tidal Flow

To verify the new bed-load transport formula for steady river flow, various reliable, existing and new field data sets (48) of bed-load transport in the sand range (up to 2,000 μm) in three major rivers have been used (see Table 2; van Rijn 2000). The measured bed-load transport rates are plotted as a function of depth-averaged current velocity in Fig. 6. The transport rates vary between 0.1 and 100 g/s/m for velocities in the range of 0.3–1.8 m/s (velocity to power of 2.5). The measured data can be roughly approximated by the following empirical expression: $q_b=0.08(u-u_{\text{cr}})^{2.5}$ with q_b=bed-load transport (kg/s/m); u=depth-averaged velocity (m/s); and u_{cr}=critical depth-averaged velocity=0.25 m/s. The fact that the bed-load transport rates of particle sizes in the range of 200–1000 μm can be represented by one trend line, shows that the effect of particle size on bed-load transport is not very large for this size range. This will be studied in more detail below.

Eq. (10) has been used to compute the bed-load transport rates for the river data given in Table 2 (depths between 3 and 10 m, d_{50} between 300 and 1,000 μm). To plot the computed results in Fig. 6, computations have been made for two extreme cases representing the measured data range: depth of 3 m and d_{50} =1,000 μm (d_{10}=500 μm, d_{90}=2,000 μm) and depth of 10 m and d_{50}=300 μm (d_{10}=150 μm, d_{90}=600 μm). Other input data are: water temperature=15°C and salinity=0 promille. The computed values are shown in Fig. 6. The bed-load transport rates for a depth of 10 m and d_{50}=300 μm are in very good agreement with the trend line of the measured values (within factor of 2). The predicted values are somewhat too small for low velocities (<0.5 m/s). The bed-load transport rates for a depth of 3 m and d_{50}=1,000 μm are in very good agreement with measured values for current velocities >0.8 m/s. It is noted that the measured transport data in the low velocity range (0.4–0.7 m/s) consist of sand in the range 200–600 μm (data from Nile River). The coarse sand data (0.6–1 mm) are in the high velocity range, see Fig. 6.

Two field data sets for tidal flow have been used to verify the bed-load transport model. During November 1964 a series of measurements was made of sediment transport in a tidal channel within the Puget Sound, Washington (Sternberg 1967). These data consisted of direct observations of the sea bed (using underwater cameras). Data were collected with an instrumented tripod. The tidal channel depth was about 23 m. The maximum tidal range was about 4 m. Bottom ripples were present (mean height of 0.015–0.024 m, mean length of 0.16 m) in a semiregular pattern with crests oriented in a cross-channel direction. The bed was

Table 2. Summary of Bed-Load Transport Rates for River Flow Conditions

Source	Number N (-)	Sediment size d_{50} (μm)	Sediment size d_{90} (μm)	Water depth h (m)	Velocity u (m/s)	Bed forms	Bed-load transport q_b (kg/s/m)
Rhine-Waal River, The Netherlands	6	1,050	1,750	9	1.4	*D*	0.1
(Van den Berg 1986)	(3)	1,050	1,750	9.8	1.55	*D*	0.18
		950	1,550	9.5	1.15	*D*	0.06
Rhine-Waal River, The Netherlands	15	530	700	4.5–5	0.45	*D*	0.002
(Gaweesh and van Rijn 1994; van Rijn 1991, 1992)	(5)	530	700		0.6	*D*	0.005
		530	700		0.82	*D*	0.031
		530	900		1	*D*	0.05
		530	1,300		1.2	*D*	0.065
IJssel River, The Netherlands	3	690	1,270	5–5.3	0.8	*D*	0.035
(Van den Berg 1986)	(1)						
Nile River, Egypt	24	200–600	300–1,600	4–6	0.33	*D*/*R*	0.0005
(Abdel Fattah 1997)	(5)				0.45		0.002
					0.6		0.006
					0.7		0.012
					0.83		0.023

Note: N=number of cases (number of groups between brackets); h=water depth; u=depth-averaged current velocity; and BF=bed forms (R=ripples, D=dunes and F=flat bed)

composed primarily of sand-sized particles which had a mean diameter of 0.43 mm. Coarse shell fragments were present in the ripple troughs. Ripple migration rates were determined yielding a mean value of about 1 cm per 5 min over a period of 40 min (12 cm/h). The observed current velocity during this period was about 0.4 m/s at about 1 m above the bed. The depth-mean current velocity was about 0.48 m/s. Using a ripple height of 0.02 m and $q_b=0.6\,\rho_s\,(1-p)\,\Delta_r\,c_r$ (with p=porosity=0.4, Δ_r=ripple height=0.02 m, c_r=ripple migration velocity=0.12 m/h), the bed-load transport is found to be about $q_b=0.00065$ kg/s/m (±50%). Eq. (10) was used to estimate the bed-load transport, using $h=23$ m, $u_{\text{mean}}=0.48$ m/s, $d_{50}=430$ μm, $d_{90}=860$ μm, temperature=15°C and salinity=30 promille, yielding $q_{b,\text{computed}}=0.00083$ kg/s/m, which is close (within 30%) to the measured value. The computed suspended transport was much smaller than the computed bed-load transport confirming that bed-load transport was dominant at this field site.

On July 11, 1968 a series of measurements was made of sediment transport on a tidal bank at the southern end of San Juan Island, Wash. (Kachel and Sternberg 1971). These data also consisted of direct observations of the sea bed (using stereo cameras). Data were collected with an instrumented tripod. The local depth was about 31 m. Bottom ripples were present with mean height of 0.01–0.05 m and mean length of 0.1–0.5 m. The bed was composed primarily of sand-sized particles which had a mean diameter of 370 μm. Coarse shell fragments were present in the ripple troughs. Ripple migration rates were determined from the measured ripple displacements over time. The bed-load transport was derived from the ripple heights and the ripple migration velocities. Two cases have been taken from the data set: Case A: measured velocity of about 0.5 m/s at 1 m above bed; depth-mean velocity of 0.65 m/s; $q_{b,\text{measured}}=0.005$ kg/s/m (±50%); Case B: measured velocity of about 0.6 m/s at 1 m above bed; depth-mean velocity of 0.78 m/s; $q_{b,\text{measured}}=0.01$ kg/s/m (±50%). Eq.

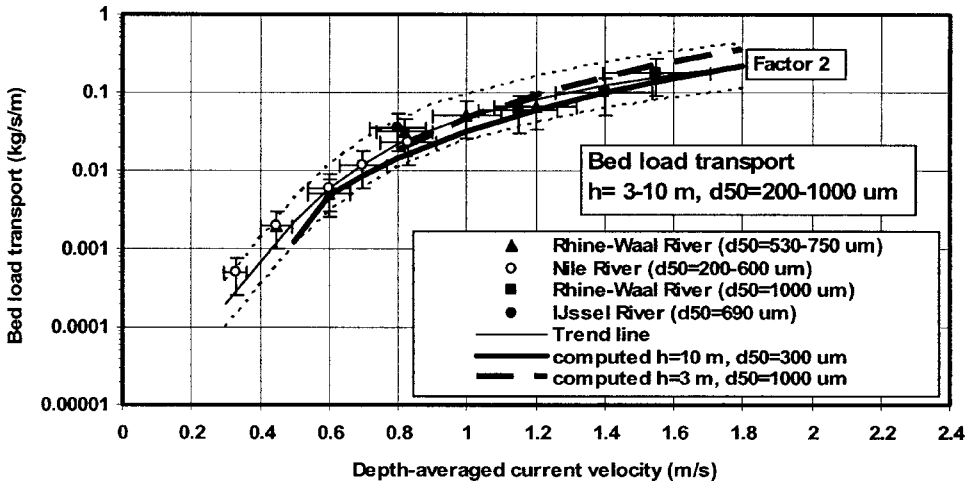

Fig. 6. Bed-load transport as function of current velocity for sand of 200–1,000 μm

Table 3. Bed-Form Transport in Shallow Depth on Spratt Sand near Teignmouth, U.K.

Depth h (m)	Sign. wave height H_s (m)	Peak period T_p (s)	Depth-mean velocity u (m/s)	Angle waves and current φ (deg)	Ripple height (m)	Ripple length (m)	Meas. bed load tr. q_b (kg/s/m)	Comp. bed load tr. q_b (kg/s/m)
1.35	0.25	6	0.55	70	0.04	0.8	0.01	0.015
1.65	0.25	5.5	0.5	70	0.05	0.7	0.009	0.010
1.65	0.35	6	0.58	65	0.11	1.3	0.042	0.025
1.85	0.35	5.5	0.55	65	0.05	0.9	0.019	0.019
1.85	0.17	9	0.62	50	0.05	0.9	0.019	0.014
1.85	0.4	6.2	0.45	100	0.07	1.0	0.016	0.0083
2.1	0.5	5.5	0.65	60	0.055	0.8	0.043	0.045
2.1	0.45	6.4	0.53	65	0.07	0.8	0.028	0.026
2.1	0.33	5.5	0.38	65	0.04	0.6	0.0061	0.008
2.4	0.3	4.7	0.55	45	0.04	0.65	0.008	0.015
2.4	0.55	6	0.47	66	0.07	1.2	0.014	0.026
2.4	0.35	5.6	0.33	105	0.06	0.65	0.005	0.0026
2.4	0.5	6.3	0.17	170	0.07	0.75	0.005	0.0012
2.65	0.63	6	0.7	65	0.075	1.0	0.051	0.06
2.65	0.17	9.1	0.73	30	0.035	0.9	0.008	0.021
2.65	0.35	9	0.55	30	0.04	1.0	0.009	0.024
2.9	0.7	6	0.65	60	0.08	1.0	0.056	0.063
2.9	0.65	6	0.33	65	0.07	1.0	0.0144	0.019
3.1	0.35	5	0.65	45	0.035	0.75	0.008	0.021
3.4	0.5	4.5	0.4	55	0.04	0.7	0.0072	0.0097

(10) was used to estimate the bed-load transport, using $h=31$ m, $d_{50}=370$ μm, $d_{90}=740$ μm, temperature=15°C, and salinity =30 promille, yielding: Case A: $q_{b,\text{computed}}=0.0046$ kg/s/m for $u_{\text{mean}}=0.65$ m/s; and case B: $q_{b,\text{computed}}=0.0105$ kg/s/m for $u_{\text{mean}}=0.78$ m/s. Both values are very close (within 10%) to the measured values.

Verification for Coastal Flow

Reliable field data of bed-load transport in coastal conditions with combined current and wave conditions are extremely scarce. Recently within the European COAST3D project, a new field data set of bed-load transport was obtained by Hoekstra et al. (2001) using instruments in a free-standing tripod. They measured (Autumn 1999) bed-form dimensions (megaripples), bed-form migration, and bed-form transport of sand with d_{50} of 300 μm (d_{90} of about 1,000 μm) in shallow depth on Spratt Sand near the town of Teignmouth, United Kingdom. The tidal range was about 4–5 m. The water depths were between 1 and 4 m. Wave and current conditions (at about 1 m above the bed) were also recorded during the tidal cycle (time-averaged values are given in Table 3).

The current velocities were measured by an electromagnetic current meter; the wave heights were derived from pressure sensor measurements. The bed-load transport rates estimated from megaripple migration and megaripple height data, using: $q_{\text{bf}}=0.6\,(1-p)\,\rho_s\,\Delta_r\,c_r$, where q_{bf}=bed form transport, Δ_r=ripple height, c_r=ripple migration velocity, and p=porosity factor=0.4.

About 75 individual data points were available, which were clustered in depth classes of 1.25–1.5, 1.5–1.75, …, 3.25–3.5 m. The original transport rates were given in m^2/s (including pores), which were converted to kg/s/m using a bulk density of 1,600 kg/m^3. Data points with roughly the same time-averaged current velocity within each depth class were averaged resulting in 20 cases, see Table 3. The variation ranges of the parameters are: about 5% for depth, 10% for wave height, 15% for velocity, 15% for bed form dimensions, and 50% for bed form transport.

The TR2004 model [Eq. (10)] was used to compute the bed-load transport based on the input data of Table 3 and $d_{10}=150$ μm, $d_{50}=300$ μm, and $d_{90}=1{,}000$ μm. The water temperature was taken as 10°C. The bed roughness was predicted by Eqs. (5)–(9). The results are given in Table 3. Fig. 7 shows the ratio of computed and measured bed-load transport as function of the relative wave height H_s/h. The agreement is quite good for H_s/h in the range of 0.15–0.25, but the computed values are too large (roughly factor of 2) for low waves with $H_s/h<0.15$. Overall, 80% of the predicted values are within a factor of 2 of the measured transport rates. Errors in computed transport rates may be caused by errors in the depth-averaged current velocity, as the current velocity was measured in one point only.

Effect of Particle Size on Bed-Load Transport

The fact that the measured transport rates of particle sizes in the range of 200–1,000 μm (see Fig. 6) can be represented by one trend line, is an indication that the effect of particle size on bed-load transport is not very large. This can also be demonstrated by showing net transport rates measured in the large-scale wave tunnel of Delft Hydraulics (Ribberink 1998; Dohmen-Janssen 1999; and Hassan et al. 1999). Fig. 8 shows the net transport rates (Tests E2, I2, and PSB1) as a function of particle size $d_{50}=210$, 320, and 970 μm ($d_{10}=130$, 180, 850 μm and $d_{90}=180$, 320, and 1,200 μm). The current velocity is about 0.25 m/s at a height of 0.1 m above the bed, the peak orbital velocity is 1.5 m/s (sinusoidal wave motion, period of 7.2 s). The measured values show a slight decreasing trend of the transport rate from 0.29 to 0.15 kg/s/m (factor of 2) for increasing particle size from 210 to 970 μm (almost a factor of 5).

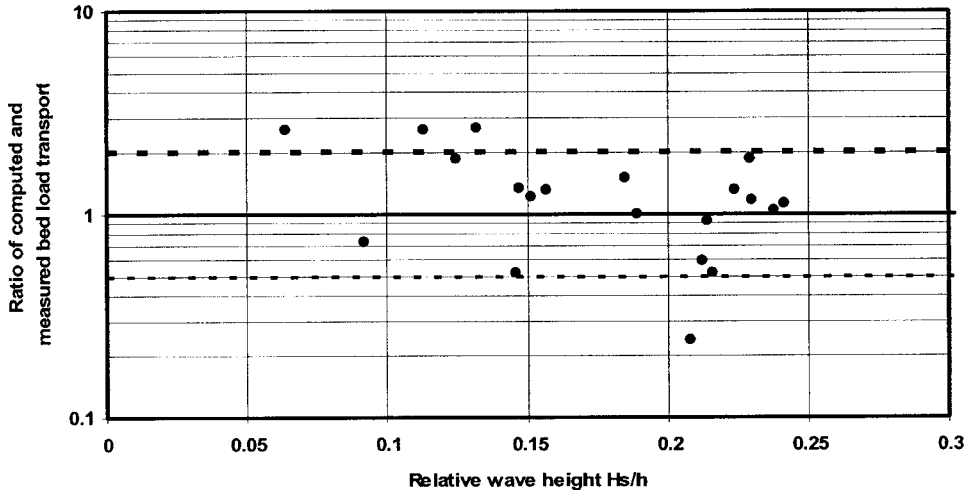

Fig. 7. Ratio of computed and measured bed-load transport rate as function of relative wave height, Teignmouth, U.K.

Computed values based on the present transport model are also shown. The measured orbital velocities were represented by using a water depth of 5 m and a wave height that gave the correct peak orbital velocities (H_s=2.5 m) as measured in the wave tunnel. The depth-averaged current velocity was set to a value (0.45 m/s) that gave the correct current velocity at 0.1 m above the bed. The wave-induced near-bed streaming (related to real waves) was neglected in the model for this case, because this effect was not observed in the wave tunnel. Temperature is 15°C and salinity =0 promille. The model predictions representing the bed-load transport (plus the suspended transport) in the wave boundary layer (of about 0.2 m) are in fairly good agreement with the measured data for particles of 210 μm, but too large (factor of 1.5–2) for particle sizes of 320 and 970 μm. The computed transport is maximum for a particle size of 320 μm and decreases slightly for larger particle sizes.

The bed-load transport model was also applied to study the effect of particle on the bed-load transport by performing a series of computations for the particle size range of d_{50}=8–2,000 μm (d_{10}=0.5d_{50}, d_{90}=2d_{50}) in coastal conditions. The water depth is h=5 m. The temperature is Te=15°C and the salinity is Sa=30 promille. Three regimes are considered:

1. No waves and u=depth-averaged longshore velocity =1 m/s;
2. Low waves with u=1 m/s, H_s=significant wave height =1 m, T_p=peak wave period=7 s, and φ=90°=angle between current and wave direction (normal to shore); and
3. High waves with u=1 m/s, H_s=3 m, T_p=7 s, φ=90°.

The computed bed-load transport rates and the suspended load transport rates (see Part 2) are shown in Fig. 9. As can be observed, the bed-load transport rate in the sand range (>62 μm) is only weakly dependent on the particle size. The bed-load transport increases slightly (factor of 2–3) for increasing particle sizes between 62 and 750 μm and then decreases. The increase of bed-load transport with increasing particle size is related to the dominant effect of the fluid drag force on the particle in comparison with gravity and friction. The bed-load transport in the silt range is approximately constant due to the effect of the silt factor [see Eq. (10)]. The weak effect of particle size on bed-load transport can also be shown from other bed-load transport formulae. For example, the bed-load transport formula of Bagnold (1966) does not have the particle size as a basic parameter. The bed-load transport formula of Meyer-Peter and Mueller (1948) is almost independent of particle size in the upper regime far beyond the critical Shields stress. The suspended load transport is discussed in Part 2, but it is clear that the bed-load transport is much smaller than the suspended load transport for particles smaller than about 300 μm.

Effect of Bed Roughness on Bed-Load Transport

The bed-load transport is only affected by grain roughness in the case of steady river flow. In the case of combined steady and

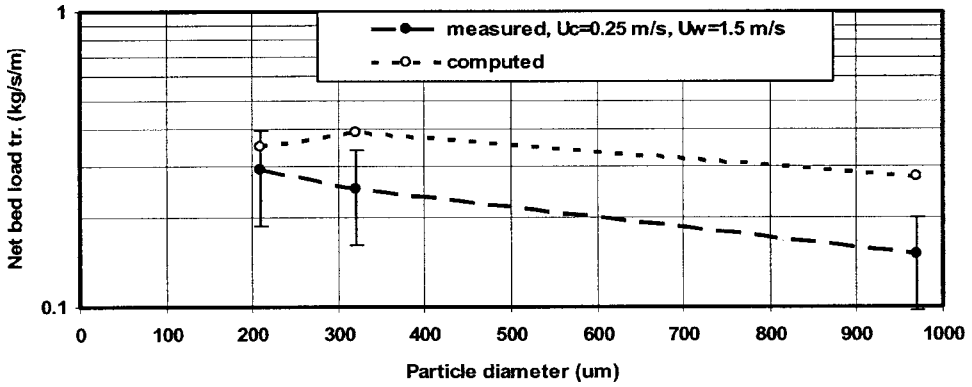

Fig. 8. Net transport in wave boundary layer as function of particle size, wave tunnel data of Delft Hydraulics

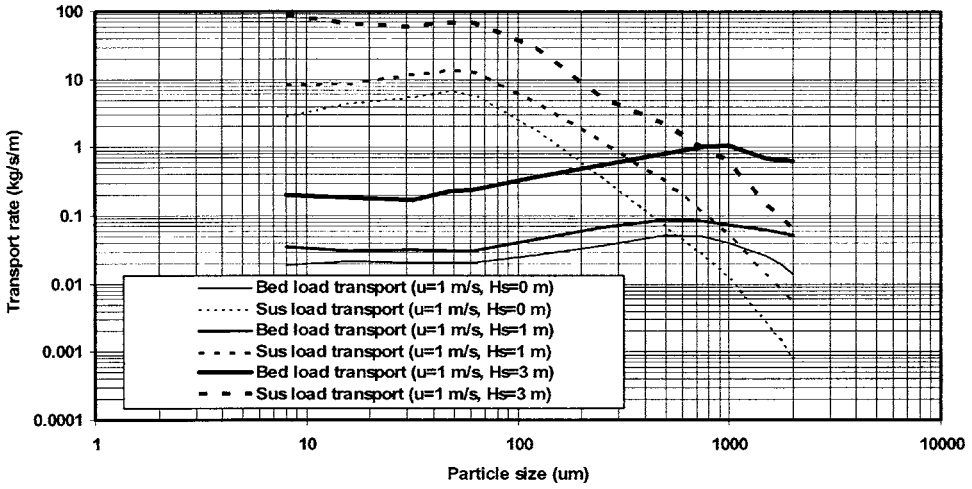

Fig. 9. Computed bed-load transport and suspended transport as function of particle size, $h=5$ m

oscillatory flow (coastal flow), the overall bed roughness may have a significant effect on the bed-load transport because of its effect on the near-bed velocity profile. As a result of the wave–current interaction and associated apparent roughness, the near-bed velocity profile is modified [Eq. (9)].

In the case of a relatively weak current and relatively large waves, the near-bed velocities are significantly reduced resulting in smaller bed-shear stresses and hence smaller bed-load transport rates. The effects are largest for a wave-current angle of 180° (opposing flow). This has been studied by a series of sensitivity computations (using a bed roughness variation of a factor of 2) for coastal flow conditions with $h=5$ m, $H_s=1$ m, $T_p=6$ s, wave-current angle=180°, $d_{10}=125$ μm, $d_{50}=250$ μm, $d_{90}=500$ μm, Te=15°C, and Sa=30 promille. The depth-averaged current velocities are in the range of 0.1–1 m/s. The current-related bed roughness value ($k_{s,c}$) has been varied by multiplying with a factor of 0.5 and 2. The wave-related bed roughness ($k_{s,w}$) was not varied. The results are shown in Fig. 10. The bed-load transport is negative (in the wave direction; against current direction) for a weak current of 0.1 m/s. In this case the asymmetric shoaling waves (based on Isobe and Horikawa 1982) yield a small net transport in the wave direction (against current direction). The bed-load transport is positive (in current direction) for velocities of 0.3–1 m/s.

The bed roughness parameter affects the near-bed velocity (u_a) and the effective friction coefficient (f'_{cw}). A larger (double) bed roughness leads to a smaller near-bed velocity and to a larger friction coefficient. The latter effect dominates for depth-averaged velocites of 0.5 and 1 m/s, resulting in larger (about 20%) bed-load transport in the case of a larger bed roughness (see Fig. 10).

The relative effect is much larger for weak currents. In the case of a current velocity of 0.1 m/s, the negative bed-load transport is a factor of 4 smaller using a smaller (half) bed roughness than that based on the default bed roughness value (−0.0005 kg/s/m instead of −0.002 kg/s/m for the default case). In absolute sense the bed-load transport is however very small for a weak current (Fig. 10). A larger wave-related bed roughness leads to a larger bed-load transport. In the case of a weak current of 0.1 m/s, the bed-load transport becomes positive (0.0013 kg/s/m) for a larger (double) wave-related bed roughness and a smaller (half) current-related bed roughness.

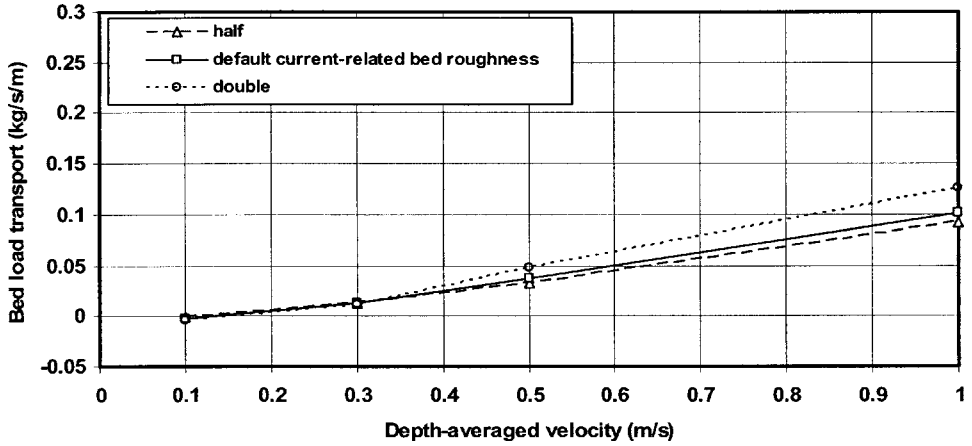

Fig. 10. Influence of current-related bed roughness on bed-load transport in coastal flow conditions (positive transport in current direction; negative transport against current direction)

Approximation Bed-Load Transport Formula

van Rijn (1984c, 1993) proposed a simplified formula for bed-load transport in current only conditions, which reads as

$$q_b = \alpha \rho_s u h (d_{50}/h)^{1.2} (M_e)^{\eta} \quad (11)$$

with $q_{b,c}$=depth-integrated bed-load transport (kg/s/m); $M_e = (u-u_{cr})/[(s-1)gd_{50}]^{0.5}$; u=depth-averaged velocity; u_{cr}=critical depth-averaged velocity; d_{50}=median particle size; h=water depth; α=coefficient; η=exponent; ρ_s=sediment density (kg/m^3); and $s=\rho_s/\rho_w$=specific density. The original α and n coefficients were found to be $\alpha=0.005$ and $\eta=2.4$ These values yield however bed-load transport rates, which are systematically too large for velocities >1 m/s and too small for velocities <1 m/s. Therefore, both coefficients were recalibrated using the bed-load transport data from Table 2, yielding $\alpha=0.015$ and $\eta=1.5$. All computed values are within a factor of 2 from the measured bed-load transport rates for velocities larger than 0.6 m/s. The measured values are underpredicted (factor 2–3) for velocities close to initiation of motion.

Following the method of Soulsby (1997), Eq. (11) can be easily extended to coastal flow (steady flow plus waves) by introducing an effective velocity u_e consisting of the steady current velocity (u) plus the peak orbital velocity (U_w), as follows: $u_e = u+\gamma U_w$. The γ value was determined by calibration using computed values of the detailed, numerical intrawave TR2004 model, yielding $\gamma=0.4$.

The new simplified bed load-load transport formula for steady flow (with or without waves) reads, as

$$q_b = 0.015 \rho_s u h (d_{50}/h)^{1.2} M_e^{1.5} \quad (12)$$

where $M_e=(u_e-u_{cr})/[(s-1)gd_{50}]^{0.5}$=mobility parameter; $u_e = u+\gamma U_w$=effective velocity with $\gamma=0.4$ for irregular waves (and 0.8 for regular waves); u=depth-averaged flow velocity; $U_w = \pi H_s/[T_p \sinh(kh)]$=peak orbital velocity (based on linear wave theory); H_s=significant wave height; T_p=peak wave period; $u_{cr}=\beta u_{cr,c}+(1-\beta)u_{cr,w}$ with $\beta=u/(u+U_w)$; $u_{cr,c}$=critical velocity for currents based on Shields (initiation of motion); and $u_{cr,w}$=critical velocity for waves based on Komar and Miller (1975) (see van Rijn 1993):

- $u_{cr,c}=0.19(d_{50})^{0.1}\log(12h/3d_{90})$ for $0.00005<d_{50}<0.0005$ m;
- $u_{cr,c}=8.5(d_{50})^{0.6}\log(12h/3d_{90})$ for $0.0005<d_{50}<0.002$ m;
- $u_{cr,w}=0.24[(s-1)g]^{0.66}d_{50}^{0.33}(T_p)^{0.33}$ for $0.00005<d_{50}<0.0005$ m; and
- $u_{cr,w}=0.95[(s-1)g]^{0.57}d_{50}^{0.43}(T_p)^{0.14}$ for $0.0005<d_{50}<0.002$ m.

Using the data of Table 3, about 75% of the predicted values are within a factor of 2 from the measured values. The inaccuracies are largest (underprediction) for relatively low u_e velocities (<0.5 m/s) close to the critical velocities. Eq. (12) describes the net bed-load transport in current-dominated conditions (longshore flows). It cannot be used to compute the net cross-shore bed-load transport in the inner surf and swash zone. For these complicated conditions the full intrawave method should be used.

Conclusions

The findings of the present study can be summarized in the following conclusions:

1. Initiation of motion of particles smaller than 62 μm on natural sediment beds (with clay and silt particles) is strongly effected by binding forces between the particles (cohesive effects); these effects can be taken into account by sediment size and packing parameters.
2. A bed roughness predictor has been developed, which can be used to determine the bed roughness in the silt and sand range from 8 to 2,000 μm; the model has been used to predict the bed roughness of the Mississippi River data showing reasonably good results.
3. Reliable field data sets of bed-load transport of sand in the range of 200–1,000 μm under steady flow conditions are available for major rivers in The Netherlands (Rhine, Waal, IJssel) and in Egypt (Nile). The bed-load transport in the current velocity range of 0.4–1.6 m/s roughly varies with current velocity to the power 2.5. The particle size in the range of 200–1,000 μm does not seem to have much effect on the bed-load transport rate in the high velocity range (>0.8 m/s). This is confirmed by bed-load transport data of wave tunnel experiments.
4. The bed-load transport rate in coastal conditions with oscillatory flow or combined steady and oscillatory flow over a sand bed can be reasonably well described (within a factor of 2–3) by time-averaging (over the wave period) of the instantaneous (intrawave) transport rates using a quasi-steady bed-load transport formula approach (TR2004 model); the effect of fluid accelerations on the instantaneous bed-shear stress in strongly asymmetric waves should be taken into account to model bed-load transport in the inner surf zone; the bed-load transport model results show good agreement with laboratory and field data for steady and oscillatory flow with sand in the range of 200–1,000 μm.
5. The bed-load transport is mainly affected by grain roughness in the case of steady river flow or quasi-steady tidal flow. The overall bed roughness has a relatively large influence on the bed-load transport in the case of weak coastal flows and relatively large waves because of wave-current interaction effects resulting in modification of the near-bed velocity profile. The relative effects are minor for relatively strong coastal flows (>0.5 m/s).
6. The effect of particle size on bed-load transport can be reasonably well represented for particle sizes in the range of about 200–1,000 μm.
7. A new simplified bed-load transport formula is proposed for river and coastal flow.

The proposed bed-load transport model can also be used for gravel and shingle. However, a deterministic approach is not appropriate for very coarse particles, because the bed shear stress will be close to incipient particle motion. In these conditions a stochastic approach is required to obtain accurate transport values (Kleinhans and van Rijn 2002).

Acknowledgments

The National Institute for Coasts and Sea (RIKZ /Rijkswaterstaat, The Netherlands) is gratefully acknowledged for providing research funds within the Generic Coastal Research Programme (VOP). Also acknowledged are the Basic Research Programme of Delft Hydraulics and the European Research Project Nos. SEDMOC, COAST3D, and SANDPIT sponsored by the European Community Research Programme. J. R. van den Berg and M. Kleinhans of the University of Utrecht are gratefully acknowledged for their critical comments on the manuscript.

References

Abdel-Fattah, S. (1997). "Field measurements of sediment load transport in the Nile River at Sohag." *Technical Rep.*, Hydraulics Research Institute, Delta Barrage, Egypt.

Bagnold, R. A. (1946). "Motion of waves in shallow water: interaction of waves and sand bottoms." *Proc. R. Soc. London, Ser. A*, 187, 1–15.

Bagnold, R. A. (1962). "Auto-suspension of transported sediment; turbidity currents." *Proc. R. Soc. London, Ser. A*, 1322, 315–319.

Bagnold, R. A. (1966). "An approach to the sediment transport problem from general physics." *Geol. Survey Prof. Paper 422-I*, Washington, D.C.

Bayram, A., Benoit, C., and Larson, M. (2003). *Equivalent roughness under sheet flow conditions* (CD-ROM), Coastal Sediment, Clearwater beach, Fla.

Bijker, E. W., Kalkwijk, J. P. Th., and Pieters, T. (1974). "Mass transport in gravity waves on a sloping bottom." *Proc., 14th ICCE Conf.*, 447–465.

Dankers, P. J. T. (2003). "A preliminary study on the hindered settling of kaolinite flocs." *Proc., INTERCOH*, Va., 221–235.

Davies, A. G., and Villaret, C. (1997). "Oscillatory flow over rippled beds: Boundary layer structure and wave-induced Eulerian drift." *Gravity waves in water of finite depth, advances in fluid mechanics*, J. N. Hunt, ed., Computational Mechanics Publications, Southampton, U.K., 215–254.

Davies, A. G., and Villaret, C. (1999). "Eulerian drift induced by progressive waves above rippled and very rough beds." *J. Geophys. Res.*, 104(C1), 1465–1488.

Delft Hydraulics. (1989). "NOGAT Offshore Pipeline; report on erodibility tests." *Rep. No. H1050*, Delft, The Netherlands.

Dibajnia, M., and Watanabe, A. (1993). "Sheet flow under nonlinear waves and currents." *Proc., 23rd Int. Conf. on Coastal Engineering*. ASCE, New York 2015–2028.

Dibajnia, M., and Watanabe, A. (1996). "A transport rate formula for mixed sands." *Proc., 25th ICCE*, Orlando, Fla., 3791–3804.

Dibajnia, M., and Watanabe, A. (1998). "Transport rate under irregular sheet flow conditions." *Coastal Eng.*, 35, p. 167–183.

Dibajnia, M., and Watanabe, A. (2000). "Moving layer thickness and transport rate of graded sand." *Proc., 27th ICCE*, Sydney, Australia, 2752–2765.

Dohmen-Janssen, M. (1999). "Grain size influence on sediment transport in oscillatory sheet flow." Doctoral thesis, Univ. of Twente, Twente, The Netherlands.

Dou, G. (2000). "Incipient motion of sediment under currents." *China Ocean Eng.*, 14(4), 391–406.

Doucette, J. S. (2002). "Bedform migration and sediment dynamics in the nearshore of a low-energy sandy beach in southwestern Australia." *J. Coastal Res.*, 18(3), 576–591.

Einstein, H. A. (1950). "The bed load function for sediment transportation in open channel flow." *Technical bulletin no. 1026*, U.S. Dep. of Agriculture, Washington, D.C.

Fredsøe, J., Andersen, K. H., and Sumer, B. M. (1999). "Wave plus current over a ripple-covered bed." *Coastal Eng.*, 38, 177–221.

Fredsøe, J., and Deigaard, R. (1992). *Mechanics of coastal sediment transport advanced series on ocean engineering*, Vol. 3, World Scientific, Singapore.

Garcez Faria, A. F., et al. (1998). "Vertical profiles of longshore currents and related bed shear stress and bottom roughness." *J. Geophys. Res., C: Oceans Atmos.*, 103(C2), 3217–3232.

Gaweesh, M. T. K., and van Rijn, L. C. (1994). "Bed-load sampling in sand-bed rivers." *J. Hydraul. Eng.*, 120(12), 1364–1384.

Graf, W. H. (1971). *Hydraulics of sediment transport*, McGraw-Hill, New York.

Grasmeijer, B. G., and Kleinhans, M. G. (2004). "Observed and predicted bed forms and their effect on suspended sand concentrations" *Coastal Eng.*, 51, 351–371.

Grasmeijer, B. T. (2002). "Process-based cross-shore modelling of barred beaches," Doctoral thesis, Univ. of Utrecht, Utrecht, The Netherlands.

Hanes, D. M., Alymov, V., and Chang, Y. S. (2001). "Wave-formed sand ripples at Duck, North Carolina." *J. Geophys. Res., C: Oceans Atmos.*, 106(C10), 22592–22592.

Hassan, W., et al. (1999). "Gradation effects on sand transport under oscillatory sheet flow conditions." *Rep. No. Z2099.10*, Delft Hydraulics, Delft, The Netherlands.

Havinga, F. J. (1992). "Sediment concentrations and transport in case of irregular non-breaking waves with a current." *Rep. No. H840, Parts E, F, G*, Delft Hydraulics, Delft, The Netherlands.

Hoekstra, P., Bell, P., Van Santen, P., and Roode, N. (2001). *Intertidal bedforms and bedload transport measurements on Spratt Sand, Teignmouth (UK)*, Coastal Dynamics, Lund, Sweden, 1028–1037.

Houwing, E. J. (2000). "Sediment dynamics in the pioneer zone in the land reclamation area of the Waddenzee, Groningen, The Netherlands." Doctoral thesis, Univ. of Utrecht, Utrecht, The Netherlands.

Houwman, K. T., and van Rijn, L. C. (1999). "Flow resistance in the coastal zone." *Coastal Eng.*, 38, 261–273.

Isobe, M., and Horikawa, K. (1982). "Study on water particle velocities of shoaling and breaking waves." *Coast. Eng. Japan*, 25, 109–123.

Johnson, B. D. (2004). "Resistance to longshore current over a rippled bed." *Proc., 29th ICCE*, Lisbon, Portugal, 1404–1416.

Kachel, N. B., and Sternberg, R. W. (1971). "Transport of bedload as ripples during an ebb current" *Mar. Geol.*, 10, 229–244.

Kleinhans, M. G., and van Rijn, L. C. (2002). "Stochastic prediction of sediment transport in sand-gravel bed rivers." *J. Hydraul. Eng.*, 128(4), 412–425.

Komar, P. D., and Miller, M. C. (1975). "On the comparison between the threshold of sediment motion under waves and unidirectional currents with a discussion of the practical evaluation of the threshold." *J. Sediment. Petrol.*, 45, 362–367.

Kos'yan, R. (1988). "On the dimensions of passive ripple marks in the nearshore zone." *Mar. Geol.*, 80, 149–153.

Li, J., Shi, W., Shen, H., Xu, H., and Eisma, D. (1993). "The bed load movement in the Changjiang Estuary." *China Ocean Eng.*, 7(4), 441–450.

Li, J., Wan, X.-n., He, Q., Ying, M., Shi, L.-Q., and Hutchinson, S. M. (2004). "In-situ observation of fluid mud in the North passage of Yangtze Estuary, China." *China Ocean Eng.*, 18(1), 149–156.

Li, M. Z., and Amos, C. L. (1998). "Predicting ripple geometry and bed roughness under combined waves and currents in a continental shelf environment." *Cont. Shelf Res.*, 18, 941–970.

Lick, W., Jin, L., and Gailani, J. (2004). "Initiation of movement of quartz particles." *J. Hydraul. Eng.*, 130(8), 755–761.

Longuet-Higgins, M. S. (1953). "Mass transport in water waves." *Philos. Trans. R. Soc. London, Ser. A*, 245(03), 535–581.

Madsen, O. S. (1991). "Mechanics of cohesionless sediment transport in coastal waters." *Proc., Coastal Sediments*, ASCE, 15–27.

Meyer-Peter, E., and Mueller, R. (1948). "Formulas for bed-load transport." *Proc., 2nd 1nt. IAHR Congress*, Stockholm, Sweden, 39–64.

Miller, M. C., Mc Cave, I. N., and Komar, P. D. (1977). "Threshold of sediment motion under unidirectional current." *Sedimentology*, 24, 507–527.

Mogridge, G. R., Davies, M. H., and Willis, D. H. (1994). "Geometry prediction for wave-generated bedforms." *Coastal Eng.*, 22, 255–286.

Nielsen, P. (1992). *Coastal bottom boundary layers and sediment transport*, World Science, Singapore.

Nielsen, P. (2002). "Shear stress and sediment transport calculations for swash zone modelling." *Coastal Eng.*, 45, 53–60.

Nielsen, P. (2006). "Sheet flow sediment transport under waves with acceleration skewness and boundary layer streaming." *Coastal Eng.*, 53, 749–758.

Nielsen, P., and Callaghan, D. P. (2003). "Shear stress and sediment transport calculations for sheet flow under waves." *Coastal Eng.*, 47, 347–354.

Nikuradse, J. (1932). "Gesetzmässigkeiten der Turbulente Strömung in Glatten Rohren." *Ver. Deut. Ing. Forschungsheft*, 356.

Peterson, A. W., and Howells, R. F. (1973). "Compendium of solids

transport data for mobile boundary data." *Rep. No. HY-1973-ST3*, Dept. of Civil Engineering, Univ. of Alberta, Alberta, Canada.
Ribberink, J. S. (1998). "Bed-load transport for steady flows and unsteady oscillatory flows." *Coastal Eng.*, 34, 59–82.
Ribberink, J. S., Dohmen-Janssen, C. M., Hanes, D. M., McLean, S. R., and Vincent, C. (2000). "Near-bed transport mechanisms under waves. A large-scale flume experiment." *Proc., Conf. 27th ICCE*, Sydney, Australia. 3263–3276.
Roberts, J., Jepsen, R., Gotthard, D., and Lick, W. (1998). "Effects of particle size and bulk density on erosion of quartz particles." *J. Hydraul. Eng.*, 124(12), 1261–1267.
Shields, A. (1936). "Anwendung der Ahnlichkeitsmechanik under der Turbulenz Forschung auf die Geschiebebewegung." *Heft 26 (Rep.)* Mitt. der Preuss, Versuchsamt. für Wasserbau und Schiffbau, Berlin.
Slaattelid, O. H., and Myrhaug, D. (1994). "Data from near-bottom measurements of flow velocity and sediment concentration in the North Sea." *Rep. No. 401515.00.01.94*, Marintek, Sintef Group, Norway.
Sleath, J. F. A. (1984). *Sea bed mechanics*, Wiley, New York.
Soulsby, R. (1997). *Dynamics of marine sands*, Thomas Telford, London.
Sternberg, R. W. (1967). "Measurements of sediment movement and ripple migration in a shallow marine environment." *Mar. Geol.*, 5, 195–205.
Sumer, B. M., Kozakiewicz, A., Fredsøe, J., and Deigaard, R. (1996). "Velocity and concentration profiles in sheet-flow layer of movable bed." *J. Hydraul. Eng.*, 122(10), 549–558.
Thorn, M. F. C. (1981). "Physical processes of siltation in tidal channels." *Proc., Hydraulic Modeling Maritime Engineering Problems*, ICE, London, 47–55.
Traykovski, P., and Goff, J. A. (2003). *Observations and modelling of large and small-scale bedforms at the Martha's Vineyard coastal observatory* (CD-ROM), Coastal Sediments, Clearwater Beach, Fla.
Van den Berg, J. H. (1986). "Aspects of sediment and morphodynamics of subtidal deposits of the Oosterschelde (The Netherlands)." Doctoral thesis, Univ. of Utrecht, Utrecht, The Netherlands.
Van der Werf, J. J. (2006). "Sand transport over rippled beds in oscillatory flow." Doctoral thesis, Univ. of Twente, The Netherlands.
Van Ledden, M. (2003). "Sand-mud segregation in estuaries and tidal basins." Doctoral thesis, Delft University of Technology, Delft, The Netherlands.
van Rijn, L. C. (1984a). "Sediment transport. Part I: Bed load transport." *J. Hydraul. Eng.*, 110(10), 1431–1456.
van Rijn, L. C. (1984b). "Sediment transport. Part II: Suspended load transport." *J. Hydraul. Eng.*, 110(11), 1613–1641.
van Rijn, L. C. (1984c). "Sediment transport, Part III: Bed forms and alluvial roughness." *J. Hydraul. Eng.*, 110(12), 1733–1754.
van Rijn, L. C. (1991). "Bed load transport measurements in the River Waal." *Rep. No. Q1300*, Delft Hydraulics, Delft, The Netherlands.
van Rijn, L. C. (1992). "Bed load transport measurements in the River Waal near Duten, near Woudrichem." *Rep. No. Q1300*, Parts II and III, Delft Hydraulics, Delft, The Netherlands.
van Rijn, L. C. (1993). *Principles of sediment transport in rivers, estuaries, and coastal seas*, Aqua Publications, Blokzijl, The Netherlands, ⟨www.aquapublications.nl⟩.
van Rijn, L. C. (2000). "General view on sand transport by currents and waves." *Rep. No. Z2899.20-Z2099.30-Z2824.30*, Delft Hydraulics, Delft, The Netherlands.
van Rijn, L. C. (2005). *Principles of sedimentation and erosion engineering in rivers, estuaries, and coastal seas*, Aqua Publications, Blokzijl, The Netherlands, ⟨www.aquapublications.nl⟩.
van Rijn, L. C. (2007). *Principles of sediment transport in rivers, estuaries, and coastal seas (update 2006)*, Aqua Publications, Blokzijl, The Netherlands, ⟨www.aquapublications.nl⟩.
van Rijn, L. C., and Havinga, F. J. (1995). "Transport of fine sands by currents and waves." *J. Waterway, Port, Coastal, Ocean Eng.*, 121(2), 123–133.
van Rijn, L. C., Nieuwjaar, M., Van der Kaaij, T., Nap, E., and Van Kampen, A. (1993). "Transport of fine sands by currents and waves." *J. Waterway, Port, Coastal, Ocean Eng.*, 119(2), 123–143.
van Rijn, L. C., Soulsby, R. L., Hoekstra, P., and Davies, A. G. (2005). *Sand transport and morphology of offshore sand mining pits (Sandpit Project)*, Aqua Publications, Blokzijl, The Netherlands., ⟨www.aquapublications.nl⟩.
van Rijn, L. C., and Walstra, D. J. R. (2003). "Modelling of sand transport in Delft3D-online." *Rep. No. Z3624*, Delft Hydraulics, Delft, The Netherlands.
van Rijn, L. C., Walstra, D. J. R., Grasmeijer, B., Sutherland, J., Pan, S., and Sierra, J. P. (2003). "The predictability of cross-shore bed evolution of sandy beaches at the time scale of storms and seasons using process-based profile models." *Coastal Eng.*, 47, 295–327.
Vanoni, V. A. (1975). *Sedimentation engineering*, ASCE, New York.
Vinzon, S. B., and Mehta, A. J. (2003). "Lutoclines in high concentration estuaries: Some observations at the mouth of the Amazon." *J. Coastal Res.*, 19(2), 243–253.
Vongvisessomjai, S. (1984). "Oscillatory ripple geometry." *J. Hydraul. Eng.*, 110(3), 247–266.
Watanabe, A., and Sato, S. (2004). "A sheet-flow transport rate formula for asymmetric, forward-leaning waves, and currents." *Proc., Conf. 29th ICCE*, Lisboa, Portugal, 1703–1714.
Whitehouse, R., Soulsby, R. L., Roberts, W., and Mitchener, H. (2000). *Dynamics of estuarine muds*, Thomas Telford, London.
Wiberg, P. L., and Harris, C. K. (1994). "Ripple geometry in wave-dominated environments." *J. Geophys. Res.*, 99, 775–789.
Wijetunge, J. J., and Sleath, J. F. A. (1998). "Effects of sediment transport on bed friction and turbulence." *J. Waterway, Port, Coastal, Ocean Eng.*, 124(4), 172–178.
Wilson, K. C. (1989). "Mobile bed friction at high shear stress." *J. Hydraul. Eng.*, 115(6), 825–830.
Winterwerp, J. C. (1999). "On the dynamics of high-concentrated mud suspensions." Doctoral thesis, Delft Univ. of Technology, Delft, The Netherlands.
Winterwerp, J. C. (2001). "Stratification effects by cohesive and noncohesive sediment." *J. Geophys. Res.*, 106(C10). 22559–22574.
Yalin, M. S. (1977). *Mechanics of sediment transport*, Pergamon, Oxford, U.K.
You, Z. L., and Nielsen, P. (1996). "Movable bed roughness in the flow of irregular waves and currents over movable beds." *Proc., Conf. 25th ICCE*, Orlando, FL., 3495–3505.
Zanke, U. C. E. (2003). "On the influence of turbulence on the initiation of sediment motion." *Int. J. Sediment Research*, 18(1), 1–15.